2006-12

Processing and characterization of NiTi Shape Memory Alloy particle reinforced Sn-In solder

Chung, Koh Choon.

Monterey, California. Naval Postgraduate School

NAVAL POSTGRADUATE SCHOOL

MONTEREY, CALIFORNIA

THESIS

PROCESSING AND CHARACTERIZATION OF NiTi SHAPE MEMORY ALLOY PARTICLE REINFORCED Sn-In SOLDERS

by

Chung, Koh Choon

December 2006

Thesis Advisor: Indranath Dutta

Approved for public release, distribution is unlimited

THIS PAGE INTENTIONALLY LEFT BLANK

REPORT DOCUMENTATION PAGE		Form Approved OMB No. 0704-0188

1. AGENCY USE ONLY *(Leave blank)*	2. REPORT DATE	3. REPORT TYPE AND DATES COVERED
	December 2006	Master's Thesis

4. TITLE AND SUBTITLE: Processing And Characterization of NiTi Shape Memory Alloy Particle Reinforced Sn-In Solders	5. FUNDING NUMBERS
6. AUTHOR(S) Chung, Koh Choon	
7. PERFORMING ORGANIZATION NAME(S) AND ADDRESS(ES) Naval Postgraduate School Monterey, CA 93943-5000	8. PERFORMING ORGANIZATION REPORT NUMBER
9. SPONSORING /MONITORING AGENCY NAME(S) AND ADDRESS(ES) N/A	10. SPONSORING/MONITORING AGENCY REPORT NUMBER

11. SUPPLEMENTARY NOTES The views expressed in this thesis are those of the author and do not reflect the official policy or position of the Department of Defense or the U.S. Government.

12a. DISTRIBUTION / AVAILABILITY STATEMENT	12b. DISTRIBUTION CODE
Approved for public release; distribution is unlimited	A

13. ABSTRACT (maximum 200 words)

In the typical packaging of a printed circuit board, the tiny-yet-critical solder joints provide both electrical connection and mechanical support for the silicon chips and their substrate. These solders are subjected to serve thermo-mechanical strains during usage and the most common failure arise from thermo-mechanical fatigue (thermal cycling). This is due to the mismatch in the coefficient of thermal expansion between the chip and the packaging substrate.

In previous work, it was proposed that reinforcement of solder by NiTi shape memory alloy particles to form smart composite solder reduces the inelastic strain of the solder and hence, may enhance the low cycle fatigue life of the solder. In this thesis, a new fabrication process for incorporating NiTi particles (10 vol.% NiTi) into Sn-In solder (80Sn-20In) using liquid phase sintering has been developed. The microstructures of the solders were characterized. The behavior of the solder joints during thermo-mechanical cycling was also characterized and the results showed that the shear stress induced in the composite solder joint is significantly reduced relative to that in the monolithic solder joint due to the generation of a back-stress associated with the B19'→B2 phase transformation of the NiTi particles during the heating part of the cycle. This causes an appreciable reduction of the total inelastic strain range during cycling.

14. SUBJECT TERMS	15. NUMBER OF PAGES
solder, shape memory alloy, NiTi, tin, indium, electronic packaging, thermo-mechanical, thermal cycling , inelastic strain	73
	16. PRICE CODE

17. SECURITY CLASSIFICATION OF REPORT	18. SECURITY CLASSIFICATION OF THIS PAGE	19. SECURITY CLASSIFICATION OF ABSTRACT	20. LIMITATION OF ABSTRACT
Unclassified	Unclassified	Unclassified	UL

NSN 7540-01-280-5500 Standard Form 298 (Rev. 2-89)
Prescribed by ANSI Std. 239-18

THIS PAGE INTENTIONALLY LEFT BLANK

Approved for public release; distribution is unlimited

PROCESSING AND CHARACTERIZATION OF NiTi SHAPE MEMORY ALLOY PARTICLE REINFORCED Sn-In SOLDER

Chung, Koh Choon
Civilian, Singapore Technologies Engineering
B.E., University of New South Wales, 1999

Submitted in partial fulfillment of the
requirements for the degree of

MASTER OF SCIENCE IN MECHANICAL ENGINEERING

from the

NAVAL POSTGRADUATE SCHOOL
December 2006

Author: Chung, Koh Choon

Approved by: Indranath Dutta
Thesis Advisor

Anthony Healey
Chairman, Department of Mechanical and
Astronautical Engineering

THIS PAGE INTENTIONALLY LEFT BLANK

ABSTRACT

In the typical packaging of a printed circuit board, the tiny-yet-critical solder joints provide both electrical connection and mechanical support for the silicon chips and their substrate. These solders are subjected to serve thermo-mechanical strains during usage and the most common failure arise from thermo-mechanical fatigue (thermal cycling). This is due to the mismatch in the coefficient of thermal expansion between the chip and the packaging substrate.

In previous work, it was proposed that reinforcement of solder by NiTi shape memory alloy particles to form smart composite solder reduces the inelastic strain of the solder and hence, may enhance the low cycle fatigue life of the solder. In this thesis, a new fabrication process for incorporating NiTi particles (10 vol.% NiTi) into Sn-In solder (80Sn-20In) using liquid phase sintering has been developed. The microstructures of the solders were characterized. The behavior of the solder joints during thermo-mechanical cycling was also characterized and the results showed that the shear stress induced in the composite solder joint is significantly reduced relative to that in the monolithic solder joint due to the generation of a back-stress associated with the B19'→B2 phase transformation of the NiTi particles during the heating part of the cycle. This causes an appreciable reduction of the total inelastic strain range during cycling.

THIS PAGE INTENTIONALLY LEFT BLANK

TABLE OF CONTENTS

THIS PAGE INTENTIONALLY LEFT BLANK

LIST OF FIGURES

LIST OF TABLES

THIS PAGE INTENTIONALLY LEFT BLANK

ACKNOWLEDGMENTS

Special thanks to Professor Indranath Dutta for his guidance and teaching throughout the thesis project, Dr Tiandan Chen for his unselfish guidance since the beginning of the project, Dr Ramesh for his assistance on the TMC set up, and my wife, Soh Peng, for the joy and sorrow. Also, to those who assisted willingly to make the NPS trip possible for the author. This work was supported by the Army Research Program.

THIS PAGE INTENTIONALLY LEFT BLANK

I. INTRODUCTION

During the operation of electronic components, solder joints experience severe thermo-mechanical cyclic loading, which leads to creep and fatigue, ultimately causing failure of the solder, and hence, the electronic package. This is due to the significant differences in the coefficient of thermal expansion (CTE) between the chip and the packaging substrate, which are joined by the solder. The solder joints must therefore be able to withstand the large thermal mismatch deformations without failure.

The failure of solders arising from a combination of temperature fluctuations and the coefficient of thermal expansion (CTE) mismatch between the chip and the PCB [3] is called thermo-mechanical fatigue (TMF). In a thermal cycling environment, the solder balls are subjected to severe thermo-mechanical cycling (TMC) conditions as the chip is periodically powered on and off or experiences heating and cooling, which can potentially result in high induced cyclic shear strains on the solder.

The situation has became more complex as ever-increasing device miniaturization, lighter weight, higher current density and multi-function ability result in greater heat generation and possibly higher temperature ranges, coupled with the need to further reduce the size of the solder balls [1, 2]. The deformation behavior is further complicated by micro-structural evolution, since solders generally operate at a high homologous temperature. Thermally induced grain growth, mechanical stress-induced grain growth and recrystallization has been observed in the high stress regions (Si/solder interface), which has been shown to be prone to fatigue cracking [3, 4, 5, 6]. In addition to the above, the formation and growth of undesirable inter-metallic compounds (IMC) between solders and substrate have a detrimental effect on the reliability of the solders. IMCs are typically very brittle and hence, enhance the propensity of fatigue cracking. In general, solders must be soft and compliant in order to reduce stresses imposed on the chip.

Figure 1 shows the schematic illustration of the shear that develops in a solder joint between a chip and substrate when the device is heated by operating current or a change in ambient temperature. As shown in the figure, the outermost solder balls are severely distorted due to the shear stress generated by the mismatch in CTE between the chip and the substrate.

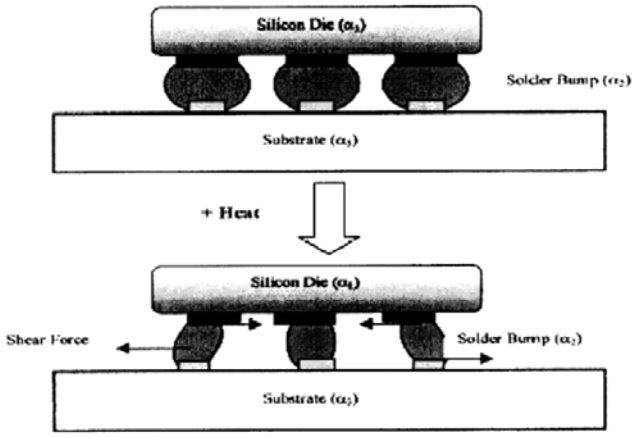

Figure 1. Thermally induced stress during normal operation (from [7])

In the past, Sn-Pb solders have been widely used in the electronic packaging industry for their low cost, ease of manufacturability and the good wetting behavior on the Cu, Ni, Ag and Au substrates. This made Pb containing solders the best candidate for electronics packaging. Moreover, there were extensive literatures established on Sn-Pb solder. However, because of various health and environmental concerns, worldwide legislation has mandated a shift to lead free solders throughout the electronic industry [8,9].

Currently, many lead free solders are used in the industry. They are namely Sn-Bi, Sn-Cu, Sn-Ag-Cu etc). Although lead-free solders are already in use, reliability issues still exist from this high thermal mismatch deformation, resulting in large solder-joint stresses and strains, which causing fatigue failure [32]. The solder balls experience a combination of creep and cyclic shear deformation, and this leads to failure of the solder at locations where the inelastic strain range is highest [10] (see Figure 1). Hence, a more positive approach to

mitigate these problems is still in progress. Hence, many consider the composite solder approach in hopes of mitigating these problems.

In the composite solder approach, reinforcements are included into the Sn based matrices to enhance the solder's fatigue life, mechanical strength and creep resistance, and in term improve its reliability. These reinforcements can be metallic or inter-metallic particles, such as Cu, Cu_3Sn, Ag, and Ni. This reinforcement approach is a rather passive solution even though improvement is expected. [13, 25, 26, 28, 29, 30, 31]

On the other hand, the "smart" or "adaptive" composite approach may be more beneficial in alleviating the TMC problem [41 - 48]. This approach consists of the incorporation of soft martensitic shape memory alloy (SMA) particles into the solder. The SMA needs to have similar yield strength as the solder so that at the beginning of the TMC, the soft martensitic SMA will deform with the solder under thermally-induced shear stress. Once the temperature is above the martensite-to-austenitic transformation temperature (A_s), the SMA particles will transform from soft martensite into hard austenite and revert to the unstrained shape, which will lead to an increase of SMA stiffness. This will impose a reverse stress on the neighboring solder matrix and thus, alleviate the strain concentration within the solder, which will consequently improve the solder reliability. This is opposite of the typical behavior of the monolithic solder which is tended to be softer at elevated temperatures.

In this project, the smart solder using Nickel-Titanium (NiTi) SMA reinforcement to the monolithic matrix of Sn-In has been assessed.

A. OBJECTIVE

The objective of this project is to fabricate a monolithic Sn-In solder as well as Sn-In solder reinforced by nickel- titanium (NiTi) shape memory alloy and conduct thermal-cycling experiment in order to understand the contribution of NiTi particles on its thermo-mechanical behavior.

THIS PAGE INTENTIONALLY LEFT BLANK

II. BACKGROUND

In this chapter, the importance of solder joint application in the electronic packaging industry is covered first. The trend of shifting into lead free solders and the types of lead-free composite solders investigated in the past recent year are discussed. Then it is followed by revealing the insights on “smart” composite solder through the reinforcement of Nickel Titanium (NiTi) Shape Memory Alloy.

A. SOLDER JOINT IN ELECTRONIC PACKAGING

In electronics packaging technology, the assembly of electronic circuits is critically dependent on the use of solder joints, which provide electrical as well as mechanical interconnections between various parts of the electronic package. The solder joints must also provide sound structural integrity, especially in surface-mount technology applications. Failure to do so will affect the integrity of the structural assembly of the electronic component as well as losing the primary function of providing electrical connection. Hence, the basic function of the electronic assembly will also be jeopardized.

With the trend moving towards higher power density [11] and higher-performance, smaller and lighter products, there has been an increasing demand for smaller component packages and/or higher pin counts. According to the Semiconductor Industry Association Roadmap, the number of input/output (I/O) interconnects in integrated circuits is expected to significantly increase over the next 10 years.

In the modern integrated circuit (IC) technology, Flip Ball Grid Array (BGA) packaging concept has received a great deal of attention, owing to its benefits to surface mount production. The BGA can provide a high number of interconnections per unit area as the area under the package can be used for the solder-sphere interconnections. It uses a less board area with smaller footprint and hence, it is also light weight [12]. In addition, they are less fragile and easier

to handle, both before and during assembly. This provides a vast advantage over the conventional lead wire bonded chip packaging approach.

The solder joint (or solder ball) of the BGA is typically placed on the substrate (printed circuit board (PCB)) and the chip placed precisely over the BGA. The solder joints are also required in order to raise the recessed I/O pads to above the passivation layer for electrical connections and for mechanical attachment of the die to the substrate [12]. Soft (ductile) solder alloys are desirable interconnect materials because of a combination of moderate electrical and thermal conductivity and a low melting point that allows the production of a metallic joint of specific geometry at moderate processing temperatures [55]. Soft solder is also excellent for alleviating TMF as it is capable of sustaining high shear strain at low stress. In addition, thermal balls under the center of the package are often used to remove heat from the device through thermal vias. These BGAs are illustrated in Figure 2. Flip chip with its advantage against convectional wire bonded microchip is shown in Figure 3.

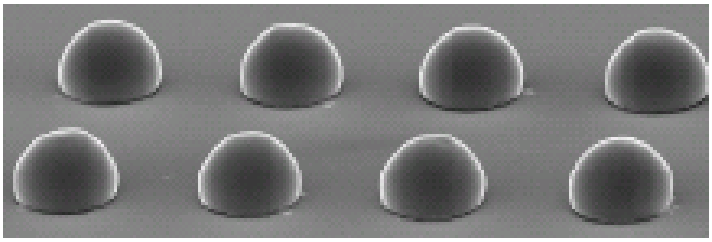

Figure 2. Arrays of tiny Solder (bumps) on the wafer (from [12])

Solder joints normally experience thermo-mechanical fatigue arising from the thermal expansion mismatch between the coefficient of the ceramic substrate (6 $x10^{-6}$ per ºC change) and PCB components (16$x10^{-6}$ per ºC change) [13]. No improvements in the CTE or replacement of the ceramic substrate have been considered because ceramic is indispensable in meeting the rigorous requirements of hermeticity and thermal and electrical conductivity, which are specifically demanded in electronic package technology.

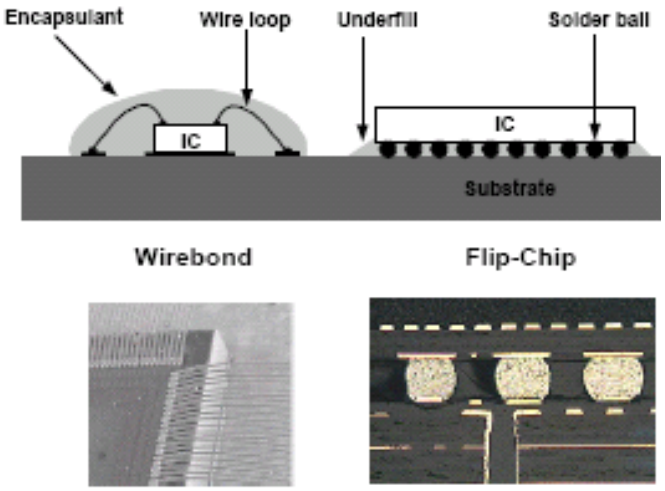

Figure 3. Interconnection in Micro-chip Packaging Technologies (from [12]) shows the number of I/O connects available for flip chip as compared to the wirebond chip

For interconnection and packaging, Pb-Sn and eutectic 63Sn-37Pb solders have been widely used in the past because of low cost, ease of manufacturability and good wettability on common electronic component substrates such as Cu and Ni [32]. These low-cost tin-lead solders have been used as joining materials in electronics for many years, and have fueled creative advanced-packaging developments such as solder-bumped flip chips, ball grid array (BGA) packages and chip scale packages (CSP). For these packaging technologies, the Sn-Pb solders, applied as tiny solder balls, were excellent as the electrical and mechanical “super glue” of the printed circuit board (PCB) assemblies.

B. LEAD FREE SOLDER

Various environmental and health issues have been raised concerning the toxicity of Pb present in the solder. Because of this, there has been a significant recent push to utilize lead free solder in electronic packaging.

In Japan, consumer goods manufactured with lead-free solders are already in production. The first Japanese lead free solder project was started in

1998 [14]. U.S. electronics manufacturers were scrambling to meet the July 1 2006 deadline set by a European Union law that barred the import of several electronic components containing lead, mercury, cadmium and other undesirable substances. The European Commission directive on the restriction of hazardous substances and similar statutes in other countries -- including one due to take effect in China by 2007 -- will affect information technology operations and technology vendors worldwide.

In the United States, where lead-free solder legislation originated, it is clear that the assemblers of electronic assemblies are forced by the necessities of the global marketplace to adopt lead-free solders. Although no such restriction is currently planned in the United States yet, U.S. users will end up buying compliant products from large manufacturers that do not want to run two assembly lines, one producing electronic components with lead and the other lead-free. Meanwhile, there are propositions in California and Massachusetts which have set a time limit to eliminate all lead from landfills [12]. Hence, all companies in the supply chain of the electronics interconnection industry worldwide are actively seeking to replace Sn-Pb solder.

Environmental and health issues have also proven that the elimination of lead (Pb) in electronic products will lead to less accumulation of electronic scrap in landfills, less electronic waste in the growing proportion of landfill solid waste, less leaching of lead into ground water sources, and minimizing landfill banned for solid waste.

In short, lead should be eventually eliminated from the electronics manufacturing. The fabrication process must ensure that the Pb-free soldered chip must be bonded to a lead-free package which must be soldered with Pb-free solder onto a lead-free PCB [12].

Currently there is no single standard Pb-free solution for all electronic interconnections. Table 1 shows the commonly used Pb free solder available in the market.

Table 1. Commonly Used Lead Free Solder Alloy (from [15])

Composition	Liquidus °C	Solidus °C	Comments
52In/48Sn	118	118	Lowest melting point solder that is feasible
58Bi/42Sn	138	138	Good thermal fatigue performance; established history
57Bi/42Sn/1Ag	140	139	The addition of Ag adds mechanical strength
77.2Sn/20In/2.8Ag	187	175	Not for use over 100°C due to In/Sn eutectic @ 118°C
86.9Sn/10In/3.1Ag	205	204	No In/Sn eutectic problem; potential use for flip-chip assembly
91.8Sn/3.4Ag/4.8Bi	213	211	Board and component metallizations must be Pb-free; Pb contamination will diminish joint strength
95.5Sn/3.8Ag/0.7Cu	220	217	Common Pb-free alloy
95.5Sn/4Ag/0.5Cu	220	217	Common Pb-free alloy
95.5Sn/3.9/Ag/0.6Cu	220	217	NEMI-promoted alloy (average composition from Indalloy #241 and #246)
96.5Sn/3.0Ag/0.5Cu	220	217	Referred to as the SAC305 alloy
96.5Sn/3.5Ag	221	221	Binary Sn/Ag eutectic alloy with history of use, marginal wetting
99.3Sn/0.7Cu	227	227	Inexpensive, possible use in wave soldering
95Sn/5Sb	240	235	Used in food equipment and refrigeration tubing. Good wettability and creep resistance
65Sn/25Ag/10Sb	233	(Melt Point)	Die-attach solder, very brittle
80Au/20Sn	280	280	Excellent mechanical strength and thermal fatigue resistance solder, used for soldering to Au
88Au/12Ge	356	356	Close to brazing alloy family, typically used in a reducing atmosphere for step soldering

1. Tin and Indium

In this project, tin and indium powder were selected to be the raw material for producing a low melting solder matrix, which could be reinforced with NiTi SMA particulates to obtain a “smart” solder. This section discusses the reasons for the selection of tin and indium.

Tin is naturally a material used for soft solder in all proportions. Combined with lead, tin alloys provide good corrosion resistance and can be used for joining most metals. Their compatibility with the soldering processes, cleaning, and most types of flux are excellent. However, pure tin cannot be applied as solder. This is because its melting point of 232°C is too high for many packaging applications, it has high surface tension than that of Pb-Sn solder, and most importantly, tin whiskers form easily under use conditions, leading to the failure of the solder [16, 17]. Tin whiskers are a crystalline metallurgical phenomenon whereby metal grows tiny, filiform hairs. The effect is primarily seen on elemental metals but also occurs with alloys. The mechanism behind metal whisker growth is not well

understood, but seems to be encouraged by compressive mechanical stresses including: residual stresses caused by electroplating; mechanically induced stresses; and stresses induced by diffusion of different metals; and thermally induced stresses.

Indium is also a popular solder for various interconnect applications due to its low melting point, low flow stress, high ductility, greater durability, excellent wetting with most metals, and good thermal fatigue characteristic. During soldering, a limited amount of inter-metallic compound (IMC) form at the solder/ substrate interface, which is considered to be a sign of good connection in the solder joints. Excellent wettability is very important for this project as it is a known fact that the wetting characteristic of NiTi and solder is poor [18].

However, an overgrowth of inter-metallic compounds (IMC) between the indium and tin will result in brittle fracture at the interface [19]. Another major drawback on using indium is its high cost and scarcity [12]. Note that pure indium cannot be applied as solder because it is too soft (low in tensile strength) to support the mechanical interconnections. Rather it may be used to enhance the ductility of the solder by adding it to a Sn based solder matrix.

Figure 4 shows the phase diagram of tin and indium. With the excellent wetting property of indium, it can able to bond tin as well as NiTi into a useful solder.

Various Sn-In solder alloys are already in used widely. SN-52In [20,21] is used as a replacement for conventional solders for application where a lower melting point is desired. The maximum use temperature for this alloy is around 120°C due to the fact that the eutectic reaction happened at 118 ºC.

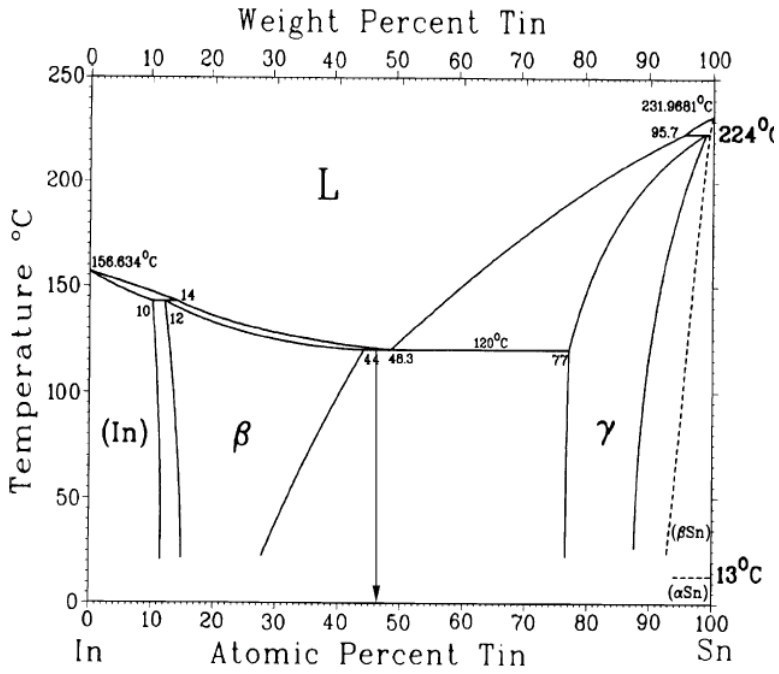

Figure 4. Phase Diagram of Tin and Indium (from [22]) shows that he eutectoid point is at 53Sn-47In with the temperature of 120°C. If liquid phase sintering of 80Sn-20In is selected, the melting point is equal to indium's (157°C).

C. COMPOSITE SOLDERS

The composite approach was adopted as reliability issues on monolithic solders exist due to the high thermal mismatch deformation, resulting in large solder-joint stresses and strains and causing fatigue failure.

In one composite solder approach, reinforcements are incorporated in the Sn based matrices to enhance the fatigue life, mechanical strength and creep resistance of the solder, and in turn, improve its reliability. Intermetallic particles such as Ni_3Sn_4, Cu_6Sn_4, Ni-coated graphite, Fe/FeSn/$FeSn_2$ and have shown that the composite approach is effective in improving the strength and creep resistance of solders by retarding grain-boundary sliding, impeding grain growth, and redistributing stresses uniformly Ag_3Sn_4 [23, 25, 26, 27, 28, 54]. This approach can provide some improvements in stress controlled fatigue life [27, 28]. In thermo-mechanical failure under strain-controlled conditions, which is a

primary deformation mode in electronic packaging, the standard composite strengthening approach has not exhibited needed improvements [24, 25]. The presence of these hard / stiff reinforcements may increase the stress levels induced into the chip, thereby making it more susceptible to cracking. Furthermore, these hard particles may accelerate damage accumulation within the solder by promoting void nucleation at the particle-matrix interfaces [26, 27, 28] as reflected in the reduced performance under strain controlled fatigue condition [29].

The feasibility of using dispersion-strengthened solders has been investigated widely and it has been shown that certain composite solders exhibit enhanced strength and other desired properties such as creep resistance and fatigue life [30, 31]. However, conventional particle strengthening of solder is plagued by many reliability problems during aggressive strain controlled thermo-mechanical cycling which are encountered during service [32]. In response to these reliability issues, there has arisen considerable interest in developing adaptive or smart solder alloys reinforced by a small amount of NiTi shape-memory alloy (SMA) particles or fiber. In this way, the solder can withstand higher externally imposed strains without a commensurate increase in the resultant stress range [33, 34, 35, 36].

1. Reinforcement Material: Nickel-Titanium (NiTi) Shape Memory Alloy

The first recorded observation of the shape-memory transformation was in the 1930s. It was not until 1962 that the effect was discovered in equiatomic nickel-titanium (Ni-Ti). Nickel-titanium alloys (NiTi) have been found to be the most useful in all SMAs. The generic name for this type of alloy is called Nitinol, which stands for Nickel Titanium Naval Ordnance Laboratory, was discovered to possess the unique property of having shape memory in 1962 [37].

The term shape-memory alloys is applied to that group of metallic materials that demonstrate the ability to return to some previously defined shape or size when subjected to the appropriate thermal procedure. Generally, these

materials can be plastically deformed at some relatively low temperature, and upon exposure to some higher temperature will return to their shape prior to the deformation. Figure 6 shows the demonstration using a thin NiTi SMA plate. Materials that exhibit shape memory only upon heating are referred to as having a one-way shape memory. Some materials also undergo a change in shape upon re-cooling. These materials have a two-way shape memory [37].

Although a relatively wide variety of alloys are known to exhibit the shape-memory effect, only those that can recover substantial amounts of strain (at least 4-5%) or that generate significant force upon changing shape are of commercial interest. To date, these have been the nickel-titanium alloys and copper-base alloys. In particular, the NiTi alloys have greater shape-memory strain (up to 8%), tend to be thermally stable and have excellent corrosion resistance.

2. Shape Memory Effect in NiTi

NiTi can exist in a two different temperature-dependent crystal structures (phases) called martensite (lower temperature) and austenite (higher temperature or parent phase). Several properties of austenite NiTi and martensite NiTi are notably different and are discussed in this section.

Figure 5 shows transformation from the austenite to the martensite phase and shape memory effect. The high-temperature austenitic structure undergoes twinning as the temperature is lowered. This twinned structure is called martensite. The martensitic structure is easily deformed by outer stress (i.e. shear due to CTE mismatch) into a particular shape, and the crystal structure undergoes parallel registry. When heated, the deformed martensite resumes its austenitic form, and the macroscopic shape memory phenomenon is seen.

There are a total of 24 possible crystallographically-equivalent habit planes of martensite. Once in the martensite form, the material is easily deformable through twinning. Particular variants grow at the expense of others to produce plastic deformation-of-shape change [27].

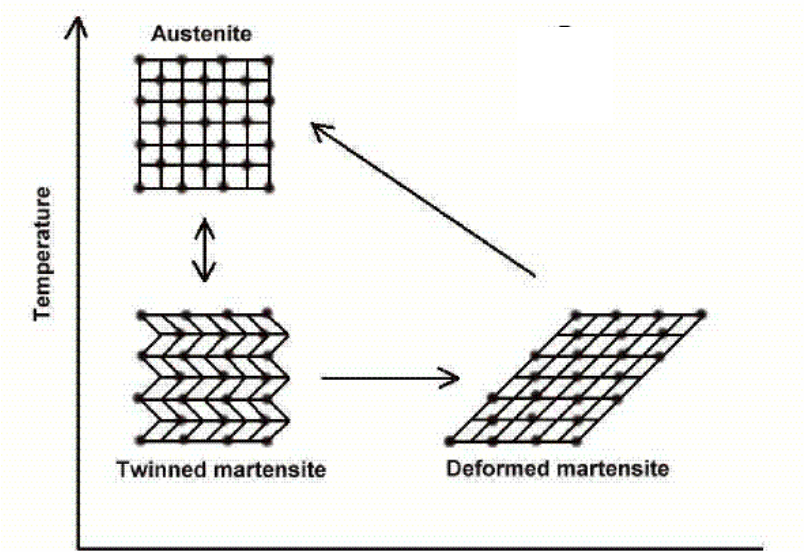

Figure 5. Transformation from the austensite to martensite phase and the shape memory effect(from[37]) along with temperature level.

While most metals deform by slip or dislocation movement, NiTi reinforced solder responds to stress by simply changing the orientation of its crystal structure through the movement of twin boundaries. A NiTi fiber will deform until it consists only of the correspondence variant (crystallographic orientation) that produces maximum strain. However, deformation beyond this (i.e. strain > 7%) will result in classical plastic deformation by slip, which is irrecoverable, and a permanent structure will result [27].

When martensite NiTi is heated, it begins to change into austenite (Figure 7.A). The temperature at which this phenomenon starts is called austenite start temperature (A_s). The temperature at which this phenomenon is complete is called austenite finish temperature (A_f). When austenitic NiTi is cooled, it begins to change into martensite. The temperature at which this phenomenon starts is called martensite start temperature (M_s). The temperature at which martensite is again completely reverted is called martensite finish temperature (M_f).

Composition and metallurgical treatments have dramatic impacts on the above transformation temperatures. From the point of view of practical applications, NiTi can have three different forms: martensite, stress-induced

martensite (super-elastic), and austenite. When the material is in its martensite form, it is soft and ductile and can be easily deformed (somewhat like soft pewter). Super-elastic NiTi is highly elastic (rubber-like), while austenitic NiTi is quite strong and hard (similar to titanium) (Figure 7. B). The NiTi material has all these properties, their specific expression depending on the temperature at which it is used. Note that super-elastic NiTi is not occurred upon application of heat but upon a reduction of stress at the temperature slight above its phase transformation temperature.

The temperature range for the martensite-to-austenite transformation, i.e. soft-to-hard transition, that takes place upon heating is somewhat higher than that for the reverse transformation upon cooling (Figure 7.A). The difference between the transition temperatures upon heating and cooling is called hysteresis. Hysteresis is generally defined as the difference between the temperatures at which the material is 50 % transformed to austenite upon heating and 50 % transformed to martensite upon cooling. This difference can be up to 20-30 °C. In practice, this means that an alloy designed to be completely transformed by body temperature upon heating (Af < 37 °C) would require cooling to about +5 °C to fully retransform into martensite (Mf).

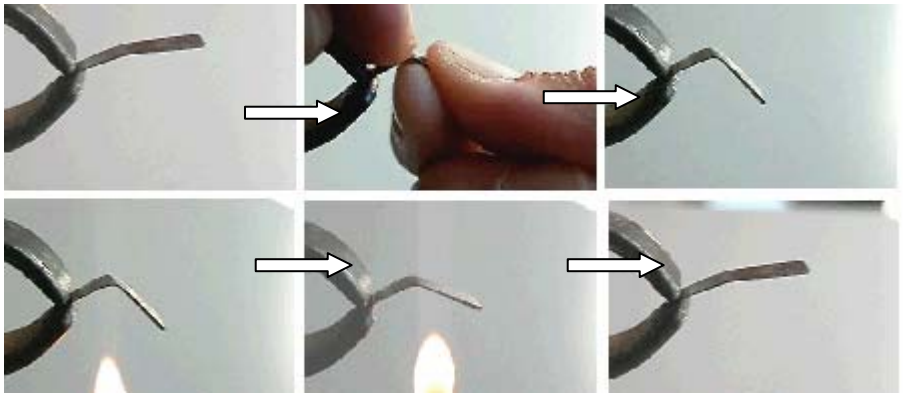

Figure 6. Demonstration of the Shape Memory Effect upon Heating (from [38]). It shows a cold work bending onto the NiTi SMA plate and by burning ir above the phase transformation temperature, the NiTi SMA returns to the original position.

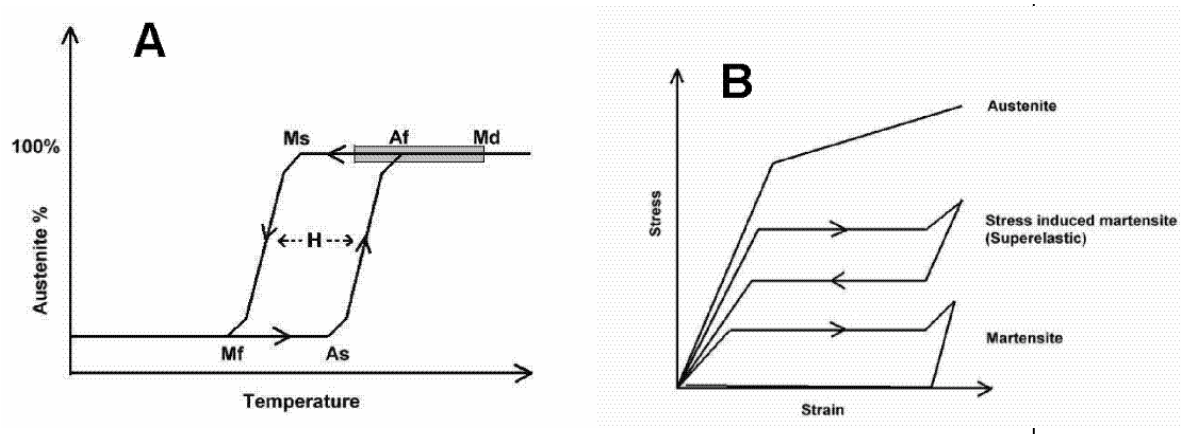

Figure 7. A) Martensitic transformation and hysteresis (= H) upon a change of temperature. A_s = austenite start, A_f = austenite finish, M_s = martensite start, Mf = martensite finish and M_d = Highest temperature to strain-induced martensite. B) Stress-strain behavior of different phases of NiTi at constant temperature

Figure 8 shows the results from Differential Scanning Calorimeter (DSC) analysis of the NiTi wires used in this project. Upon heating, the monoclinic martensite (B19'-phase) transform completely to the BCC austenite (B2-phase), after a single exothermic peak at 42ºC. Upon cooling from the 85ºC, at the first peak at 22ºC, the wire transforms first to a mixture of rhombohedral-martensitic (R-phase) and B19'-phase, prior to the martensitic transformation. The second peak during the cooling, at -35ºC, represents the complete transformation of the R-phase to B19'-phase, thus producing a single-phase B19' structure. The thermo-elastic martensitic transformation causing the shape recovery is a result of the need of the crystal lattice structure to accommodate itself to the minimum energy state for a given temperature and stress [28].

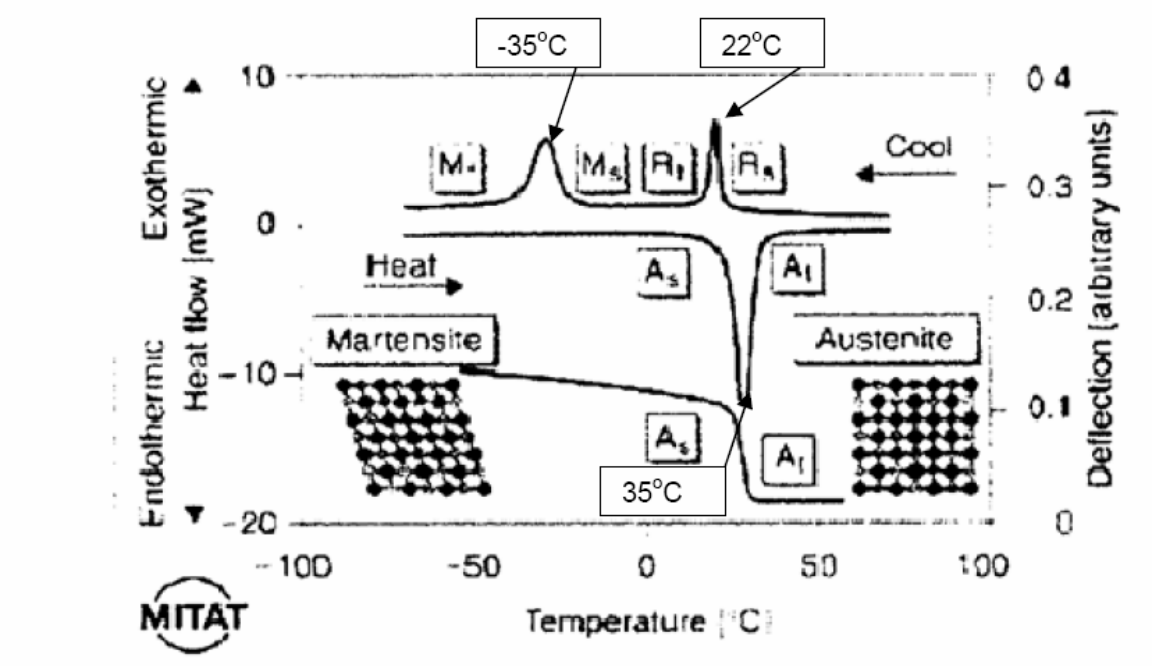

Figure 8. DSC curves of NiTi wire. Note that upon cooling the wire transforms to R-phase prior to the martensitic transformation. Upon heating, the A_s and A_f temperatures are similar, as the monoclinic martensite transforms to the cubic austenite, (from [39])

3. Composite Solder with NiTi Reinforcement

The idea for a SMA reinforced solder is that at low temperatures, SMA fiber/particles are in the soft martensitic state and can, during the raising of the temperature, plastically shear with the solder, which causes the displacement difference between the chip and the PCB. Then, when the working temperature of the chip crosses the martensite-to-austenite transformation temperature, the SMA reverts to the original shape and the transformation strain induces a backstress on the matrix, acting as a reverse eigen-strain and reducing the creep rate at locations where the inelastic strain accumulation is high. Thus, by reducing the inelastic strain in regions near the substrate, the process improves the fatigue life of the solder [5]. This behavior can be seen in Figure 9. The same analogue is used for NiTi particulates in the monolithic solder.

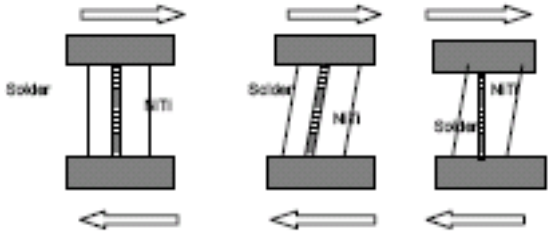

Figure 9. NiTi Martensite to Austenite Transformation Placing solder in the reverse shear ([40])

Since early 1990s, there were attempts to develop ‘‘smart’’ solder alloys with reinforcement of NiTi particulates [10, 18, 33, 34, 35, 36, 40, 41, 42, 43, 44, 45, 46, 47, 48,]. These attempts had focused on exploiting the super-elastic properties of austenitic NiTi to reduce the stresses in the solder matrix immediately adjacent to reinforcements [41 -46]. The limited mechanical property data available on these materials have suggested that super-elastic NiTi reinforcements simultaneously enhance stiffness and ductility of the solder [46], although a clear mechanistic rationale for this behavior and its role on TMC behavior is unknown. Austenitic NiTi is much stiffer and stronger than the solder; it is unclear whether the load level needed for austenite-to martensite transformation for super-elasticity in NiTi can be achieved in the solder matrix. In addition, the super-elasticity typically occurs over a relative small temperature range slightly beyond the austenite finish temperature (A_f) [37]. Hence, this phenomenon may not cover the significant part of the TMC conditions of the electronic components. Furthermore, obtaining a uniform particulate distribution has proved difficult due to poor wetting between NiTi and liquid solder, even following coating of the particles with Cu or Ni [42-44]. The electro-less Ni and Cu coatings have been used extensively to promote the wetting of NiTi, with the solder also providing a diffusion barrier to prevent the formation of inter-metallics at the interface between solder and reinforcement. This layer behaves as a sacrificial layer, leading to the absence of the intermetallic formation [42-44]. These wetting characteristics have been shown to deteriorate with time and temperature, as the solder is exposed to high homologous temperatures during

thermo-cycling. This suggests that the coating approach may not be suitable for microelectronic applications, where multiple reflows are common.

More recently, uniformly distributed martensitic NiTi particle reinforced solder composites have been produced without pre-coating the particles, using an aggressive HF-based flux to de-oxidize the particulate surface [47]. Furthermore, using single fiber composite (SFC) joints, it has been shown that reinforcement by martensitic NiTi significantly reduces the average inelastic strain imposed on a joint during TMC, as compared with monolithic solder [47]. It has been proposed [18, 47] that the soft martensitic NiTi deforms in conjunction with the solder matrix as the joint is loaded in shear during TMC, followed by snapping back to their original shape at the martensite-to-austenite transformation temperature, thus placing the solder matrix next to the particles in reverse shear. By imposing a back stress, the reverse shear would reduce the forward inelastic strains (plastic/creep) in the solder and improvements in resistance against creep, leading to longer fatigue life.

The attempt to produce NiTi reinforced solder balls formed by reflowing the composite solder paste. Although it noted that the wetting of the NiTi by liquid solder was reasonably good with no large-scale clustering of particulates and no noticeable voids nucleation, large portion of the NiTi particles was rejected from the solder during re-flow, implied that the well-distributed NiTi particles was not easily achieved [18].

Follow-on experimental work on martensitic NiTi/solder SFC joints [35, 47] has verified the production of a back stress associated with the martensite-to-austenite transformation, and modeling work has shown that this stress is large enough to decrease the solder creep rate and strain range significantly, and is thus able to delocalize displacement-limited strains within the joint. However, the composite solder paste with NiTi SMA particulate reinforcement showed rejection of NiTi particles during reflow with the composite paste in molten state.

Nevertheless, it did demonstrate that the wetting of the NiTi particles by liquid solder is reasonably good by the fact no large scale clustering of particulates is noted [10].

In this year, similar work [48] was done on the monolithic solder 95.5Sn-3.8Ag-0.7Cu reinforced by NiTi fiber had clearly showed the benefits of SMA. The benefits were the sudden drop in inelastic shear strain at SMA transformation temperature of about 40°C - 50°C during heating and also able to withstand higher shear stress at the same temperature region. The work also showed evidence of reverse deformation in the solder commensurate with the NiTi phase transformation. Most importantly, it showed that the substantial strain concentration at the NiTi reinforcement extremities was unlikely to be as significant as the analytical prediction.

Finally, the CTE of the solder itself could be altered to reduce the thermal stresses that could develop with low-CTE substrates by adjusting the volume fractions of the reinforcements. A composite solder should not be made so strong or rigid that failures will take place primarily in the components [13]. Hence, a small volumetric fraction of NiTi SMA shall be used on the monolithic solder.

D. FABRICATION OF SOLDER (LIQUID PHASE SINTERING)

In this project, liquid phase sintering (LPS) was adopted as the fabrication process to produce solders containing well distributed NiTi particulates, in order to alleviate the possible rejection of the NiTi particles during melt-fabrication [40].

Corbin el at. [49] fabricated Sn-Bi solder by LPS and obtained a homogeneous structure with good properties. To date, however, there is no written literature on fabrication of Sn-In by LPS. In the following, the mechanism of LPS is outlined.

Liquid phase sintering (LPS) is a sintering process in which a liquid phase co-exists with a particulate solid at the sintering (elevated) temperature [50]. LPS offers rapid densification kinetics. It is much faster than solid state sintering, due

to the higher diffusivity and mass transport in liquids. Liquid capillary action (equivalent to a large external pressure) aids in rearrangement of the particles in early stages of sintering. Also, the enhanced reactivity of the liquid with the solid results in densification due to a rapid dissolution-transport-precipitation phenomenon. LPS is practiced widely, both for consolidation of metallic and ceramic powders. Consolidation of metallic powders through LS is an attractive, cost effective method of producing near-net shape components for automotive and consumer markets.

The densification kinetics of LPS does not depend on lattice diffusion, except in the very last stage of the predominantly solid-solid contacts between particles. Thus even covalent solids, that normally have very low diffusivity, can be sintered.

In the LPS process, three overlapping stages are usually defined for a typical case. The stages are as follows:

- Rearrangement
- Solution Re-precipitation
- Solid state sintering

In this project, the re-arrangement stage was used with certain degree of solution re-precipitation and the solid state sintering phase was not used.

1. Rearrangement Stage of LS

The sample consisting of a high melting majority phase and a low melting minority phase (10-30 vol. %) is first packed (pelletized) to a green density of at least 60%. It is then subjected to a sintering temperature which is slightly above the melting point of the minority phase. This allow the minority phase to be melt and wet the majority phase, enabling particle rearrangement to occur by surface tension.

During the rearrangement stage, the mixed powder of Sn/ In is subjected to rapid shrinkage under capillary pressure from high-curvature indium liquid

necks betweens solid grains. The molten indium would travel and wet around the tin grains and NiTi SMA particulates by the action of capillary pressure with the solid tin and NiTi particles slide over one another.

As rearrangement proceeds, the elimination of porosity gradually increases the compact viscosity and results in a decrease in the densification rate. Finer spherical particles rearrange more easily than irregular particles.

The rearrangement step can be prevented by strong solid-state bonds formed during heating (i.e. before rearrangement), high green density compaction, and interlocking and/or irregular particles

Rearrangement is accelerated by low wetting angle, small particles (resulting in higher capillary forces), dihedral angle (tangential angle between two solid particles, minimal solid-solid contact (i.e. low initial green density, loose powder structure and little solid state sintering), and high solubility of solid in liquid.

The rearrangement stage is not only the shortest (or the fastest in terms of the densification rate) stage of LPS, but also the most significant and characteristic stage of LPS. After the melt forms, the major portion of densification occurs in a few minutes (2-5 min) and the rearrangement stage is usually completed within 10 minutes of the low-viscosity melt formation.

The dramatic changes within the powder compact during the rearrangement stage involve [50]:

- liquid spreading,
- capillary attraction,
- particle sliding and coalescence,
- particle disintegration-fragmentation,
- diffusional homogenisation,
- rearrangement between particles AND clusters of particles

By spherical volume computation, it was estimated that about 7% of indium is required to fulfill the formation of 1 μm thick of indium layer around the spherical tin grain. Thus, in this project, 10%-30% Indium was added to the pure tin to compensate for indium loss during LPS. Certain quantity of molten indium was expected to be lost via the vent holes from the graphite die.

2. Solution Re-precipitation Stage of LS

This stage is dominant when rearrangement is complete. It is active at all stages of LPS. The following phenomena are observed during the solution re-precipitation stage [50]:

- Contacts under pressure and curved surfaces dissolve preferentially.
- Dissolved matter is transported away due to a concentration gradient.
- The particle centres approach if the dissolved matter originates between the contacting grains.

Densification and growth of the particles of the solid phase in the solution-re-precipitation stage proceeds primarily by contact flattening, due to preferential dissolution of the contacts under stress. Therefore, the application of external pressure in LPS accelerates densification through faster dissolution re-precipitation, in addition to the faster rearrangement under external stress. However, the accompanying dissolution of small grains and re-precipitation on large grains during the solution re-precipitation stage leads primarily to grain growth without densification.

THIS PAGE INTENTIONALLY LEFT BLANK

III. EXPERIMENTAL WORK

A. LIQUID PHASE SINTERING

1. Experimental Materials

a. Tin and Indium

Both tin and indium powders were from Sigma Aldrich 99.8% pure tin (325 mesh; <44 μm) and Alfa Aesar 99.9% Indium (325 mesh; <44 μm).

Indium powder is self-passivating due to the rapid formation of the oxide layer on the surfaces of the powder. Typically a thickness of 80-100 Angstroms of oxide resides on the surface. Prior to using indium, it is recommended that this oxide layer be removed and return any unused indium to storage under nitrogen or argon. Initially, etching tin and indium separately was employed using methanol solution containing certain amount of hydrochloric acid and nitric acid for time duration of not more than 5 minutes. However, high contamination (oxide) was found in the powder following chemically etching the indium powder. The powder tended to conglomerate severely after etching and drying, forming slugs of indium particles rather than a free flowing powder.

Therefore, the etching method was abandoned and the final approach was to deform the mixed Sn/In powder moderately. It is discussion in section Chapter III A.2.

b. NiTi

The NiTi powder with less than 38 μm-sized particulates was prepared from the commercial NiTi wires of 1 mm diameter from Dynalloy Corporation.

The surfaces of the 1-mm thick NiTi wires were first ground with 320-grit silicon-carbide sandpaper in order to remove the oxide layer. After this, they were cold-rolled into strips of approximately 0.2 mm thickness. The

hydrogen embrittlement process was performed on the NiTi strips to assist in the hand grinding process. An electrochemical cell was produced in order to cathodically charge the NiTi with hydrogen, using a normal of sulfuric acid (H_2SO_4) and very little amount of Thiourea with a 0.5-mm-diameter platinum wire in coil shape as anode and the NiTi wire as cathode. Thiourea was an organic compound which acts as a catalyst poison on hydrogen absorption reaction. A DC power supply of 5 V with a current of 0.2A was used to allow hydrogen to diffuse into NiTi strips [51]. Figure 10 shows the schematic diagram of the hydrogen embrittlement setup.

After hydrogen-embrittlement process, the NiTi strips were carefully ground to powders and were passed through sieve of the mesh size 38-μm. The grinding was done in a mortar and pestle. Finally, the NiTi powder was vacuum annealed at 550°C for an hour to alleviate the hydrogen embrittlement and the shape memory effect was checked using Differential Scanning Calorimetry (DSC).

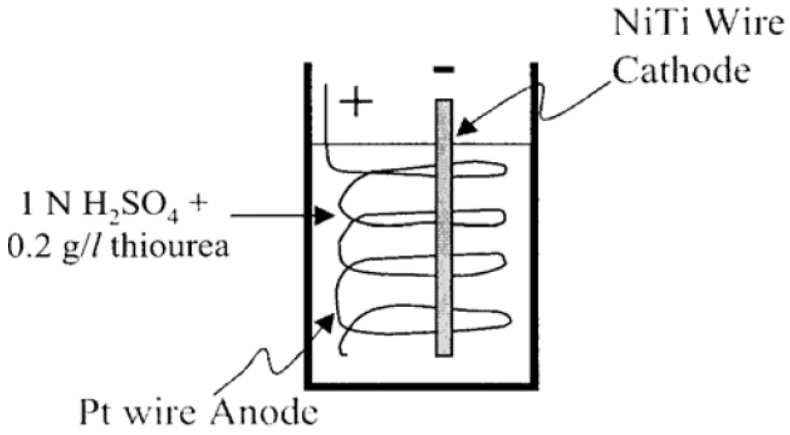

Figure 10. Hydrogen embrittlement setup, from reference [18]

2. Mixing and Powder Compact

The two metallic powders were mixed together by vigorously shaking in a small container for about 15 mins. The mixed powder was then hand-ground in a mortar and pestle for another 15 mins. This grinding was gently performed in an

argon filled glove bag/box. The intention of grinding the powder was to “peel off” or deform the oxide layer on the indium and tin surfaces to expose the non-passivated surfaces for sequence powder compacting and liquid phase sintering. Since there was no oxygen to react with the surfaces, further oxide did not form on the new surfaces. Excess powder was returned into the vacuum flask.

The well mixed Sn-In powder was poured into a graphite die and compacted in between two copper rods of diameter 5.8-mm. The graphite die was a cylindrical shape with a through hole of diameter 5.8 mm along its centerline. The solder sample was pre-packed into pellet form with an applied pressure of about 35 MPa with excess indium powder sprinkled on the interface between the solder and the copper rods to enhance the interface joint. Then, the applied pressure was reduced to 3 MPa in preparation of the LPS. The purpose of lowering the applied pressure was to minimize the loss of excess indium as well as to allow particle rearrangement during the LPS. This process produced a joint with the same diameter as the copper rods and the graphite die (diameter of 5.8 mm), and a thickness of about 0.2 mm. Together, the two copper rods with the solder joint in between is referred to as a single joint shear (SJS) sample [52].

The composite solder was prepared in the same way as the monolithic solder. The three metallic powders were mixed in the small container and hand-grounded in the mortar and pestle and compacted in the same way as the monolithic sample.

3. Making of Solder Joints

The two-piece cylindrical furnace was pre-heated to 170°C separately with the thermocouple, which was fed into the temperature controlled at the center of the furnace. After the desired temperature was reached, the furnace was immediately shifted to the SJS sample location. The SJS sample was still constantly subjected to an applied pressure of 3 MPa and was residing in an argon filled container. The SJS sample was heated up to 162°C in about 15 to 20 mins. Once the sample temperature reaches 162°C, the furnace was removed

and the SJS sample was cooled to room ambient using forced convection generated from a blower/fan. After the SJS sample was cooled down, the graphite die was carefully removed to ensure the SJS sample was not damaged. Figure 11 shows the sample partially capsulated by the graphite die which holds the SJS during LPS, as well as the SJS sample itself.

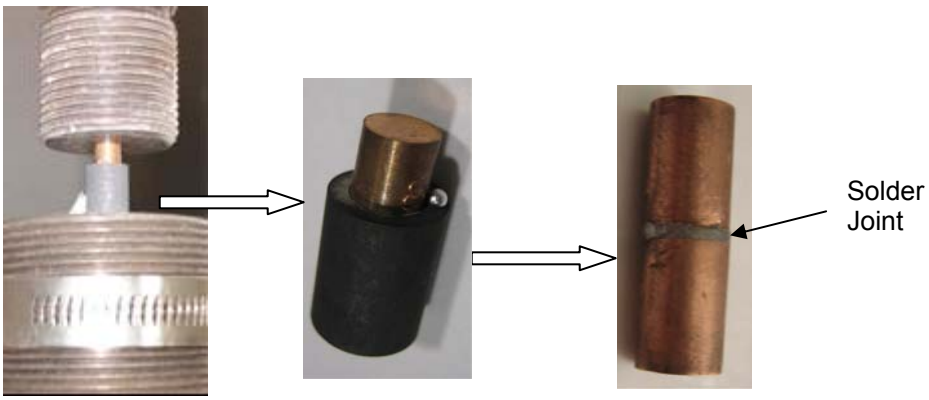

Figure 11. From sample under applied pressure, sample in the graphite die (with excess indium squeezed out) to the sample alone

4. Apparatus Set Up

The main apparatuses used for LPS were the furnace and SATEC unidrive load system. Figure 12 shows the apparatus setup for LPS.

The furnace was a two piece cylindrical shaped heater which connected to a Eurotherm model 808 temperature controller. The desired temperature was manually set in the temperature controller and the connecting thermocouple fed back on the actual temperature of the SJS sample location to the temperature controller. Based on the temperature difference, the temperature controller supplied the corresponding electrical power to the furnace in term controlling the temperature in the furnace.

The SATEC unidrive load system was controlled by a personal computer. The compaction pressure setting, time duration and its desired rate were input into the computer.

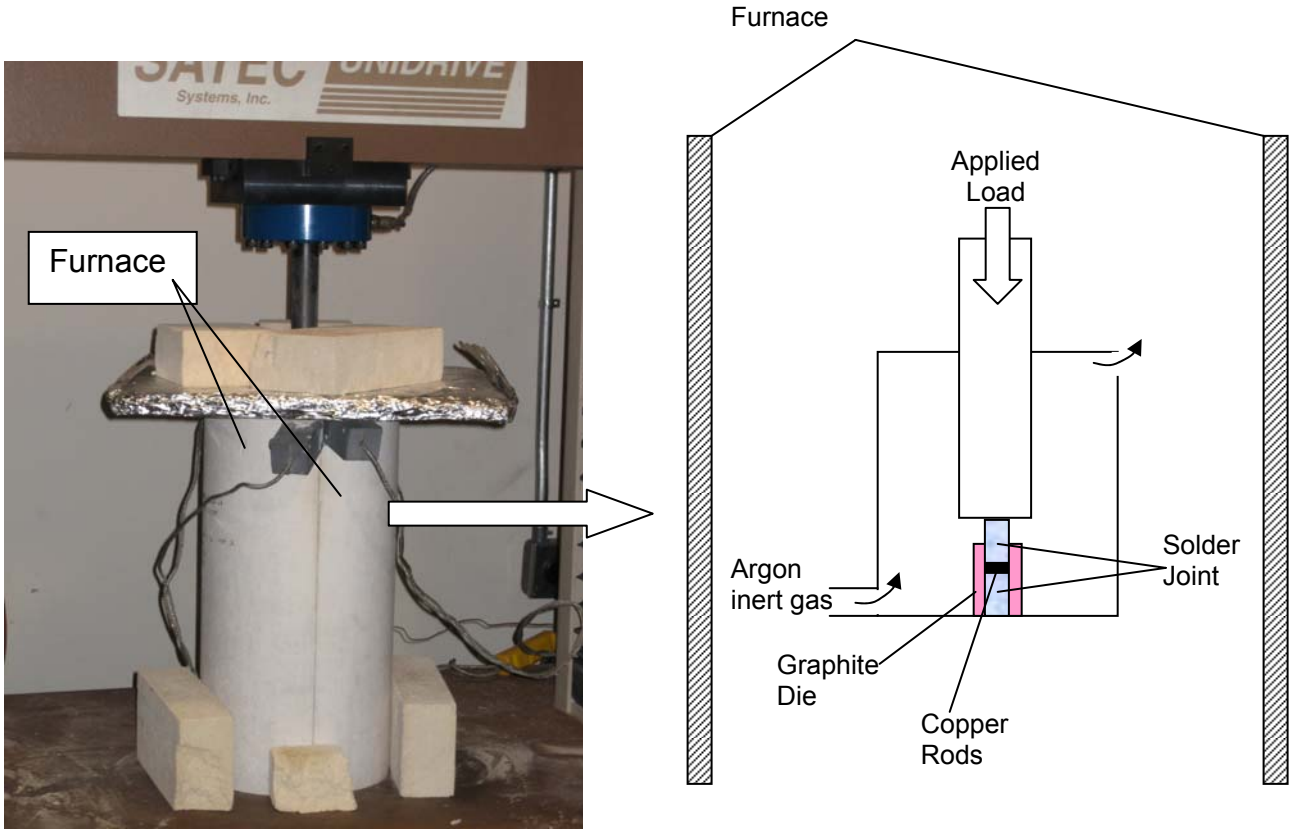

Figure 12. Liquid Phase Sintering Apparatus

B. THERMAL CYCLING TEST

The thermo-mechanical behavior of the SJS sample was measured using an experimental apparatus (fixture), which consisted of a TMC frame [53, 54] and a temperature controlled chamber similar to the apparatuses used in earlier work [52]. Figure 13 shows a schematic diagram of the bimetallic fixture (TMC Frame). This fixture was designed to shear-stress the samples. After the SJS was secured in the bimetallic frame of the fixture, it was subjected to temperature cycling of -25 ºC and 125 ºC with a ramp rate of 7.5 ºC and dwell time of 7 mins. Figure 14 shows the standard temperature-time profile which the SJS sample had undergone.

This temperature profile exhibits the actual temperature-time profile that the solder experiences during the operation of an electronic component. Modern interconnection technology must be designed to dissipate the maximum amount of heat and prevent the maximum power device operating temperature, usually 125ºC for a semiconductor device, from being exceeded [55].

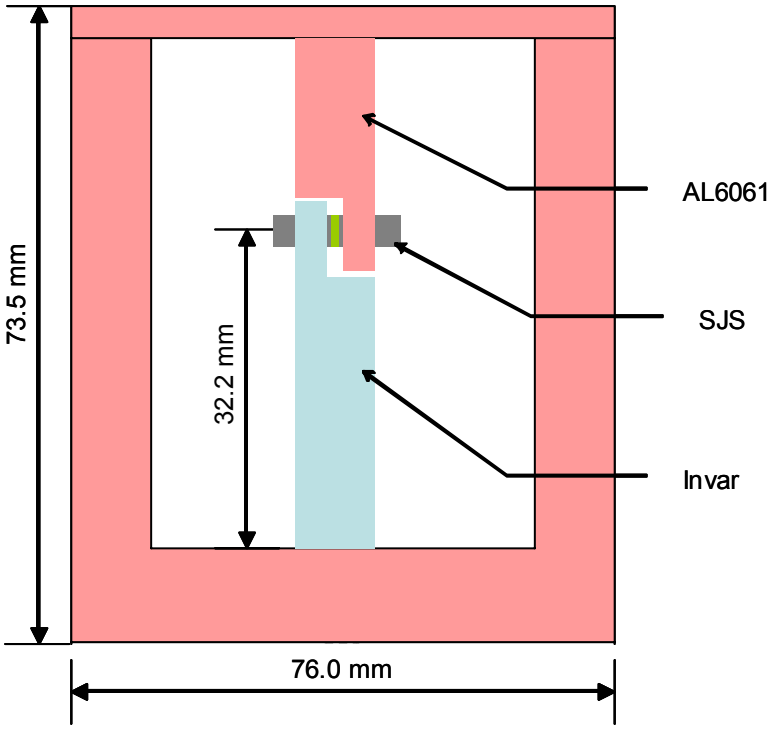

Figure 13. Bimetallic frame with specimen inserted, after reference [26]

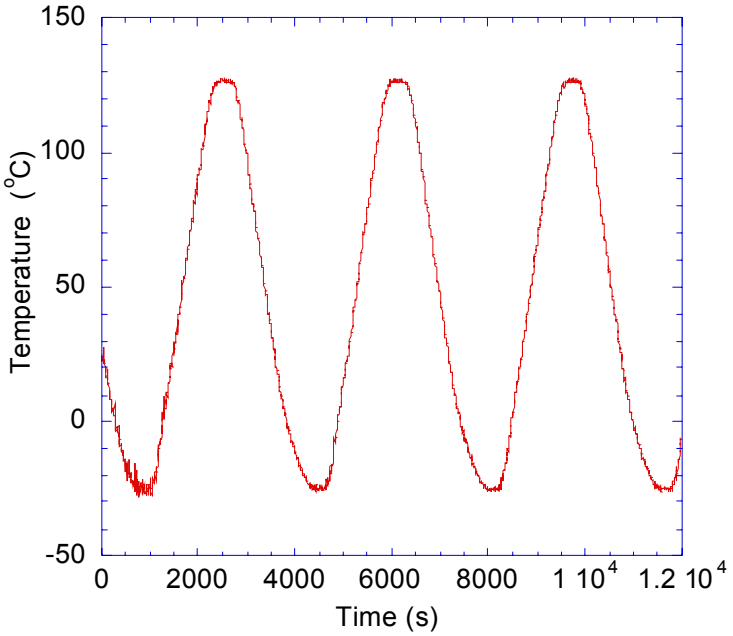

Figure 14. Standard Temperature Profile for all TMC tests

The frame was made up of mainly Al 6061 and a short column of invar. The SJS sample was secured horizontally between the Invar and Al 6061 with one end of it attached to Al 6061, and the other end attached to Invar (refer to Figure 13). Invar is a nickel-iron alloy which was known to possessing a very low rate of thermal expansion (α_{Al} = 2.28 x10^{-5} / K^{-1} and α_{Invar} = 7.20 x10^{-7} / K^{-1}).

As the frame was subjected to increasing temperature, the Al and Invar expand based on their CTE, α, and produce a relative displacement given by [52].

$$\delta_{thermal} = \Delta\alpha \, L_{Invar} \, \Delta T$$

Where $\delta_{thermal}$ = deflection due to thermal changes

$\Delta\alpha$ = CTE difference between invar and AL6061

L_{Invar} = length of the Invar and Al 6061 fixture (32mm)

ΔT = temperature change from ambient

The temperature reading was taken from a thermocouple placed inside Invar column in vicinity of the SJS location. By virtue of the large differences in CTE between the two members of the frame (α_{Al} = 2.28 x10^{-5} / K-1 and α_{Inv} = 7.20 x10^{-7} / K-1), the invar portion of the column expanded or contracted more than the rest of the column, and hence, a shear is applied onto the SJS. If the solder was completely compliant and did not resist shear, the difference in expansion mentioned above would give the displacement of the joint in shear. This would mean that the solder was very ductile. However, because the solder resisted the shear by pulling the copper rod back towards the original position, this caused mechanical deflection in the upper beam of the frame. This deflection was measured by four strain gauges forming a Wheatstone bridge-type. The strain gauges were placed in pairs on the beam on either side of the upper beam. This arrangement allowed compensation for thermal induced strains, and measure only the mechanically induced strains on the upper beam.

The mechanical deflection and the force imposed on the upper beam of the frame was known with the calibration curve in Figure 16. This was derived using MTS load system to provide the magnitude of the deflection and load with the corresponding reading from strain gages. Three separate measurements was made and the relationship equation shown in the figure was the averaged of the three sets of data.

The solder joint shear strain had been determined by the following method. The computation was done for every time step of 5 seconds. The room ambient condition was taken as the reference temperature level for zero strain. The strain gauge readings from the thermal cycling experiment comprised the strain readings from just the frame hypothesis and the solder. Hence, the frame baseline response had to be subtracted from the strain gauge reading.

Solder Strain Gage Reading = Strain Gage Reading – Frame Gage Reading

The baseline response of the frame consisted of the strain gauge reading as the frame was cycled thermally without placing a SJS sample in it. This

relationship is shown in Figure 15. It was obtained by running the thermal cycling test on the frame only. Note that only the gradient in the equation stated in Figure 15 is of interest in the computation. The frame baseline was assumed to be kept constant regardless of the SJS signal.

During thermal cycling of the frame as an assembly with the SJS sample, its deflection due to CTE difference, $\delta_{thermal}$, is equal to the sum of the deflection of the frame, δ_{mech}, and the deflection of the solder deflection, δ_{solder},:

Deflection $$\delta_{thermal} = \delta_{solder} + \delta_{mech} = t(\gamma_{el} + \gamma_{pl}) + \frac{\tau A}{K} = \Delta\alpha \ \Delta T \ L_{In\,\mathrm{var}}$$

Shear Strain $$\gamma_{mech} = \frac{\delta_{mech}}{t} \ ; \qquad \gamma_{thermal} = \frac{\delta_{thermal}}{t} \ ; \qquad \gamma_{solder} = \gamma_{thermal} - \gamma_{mech}$$

Where t is the thickness of the solder, and A is the cross-sectional area of the solder joint.

The difference in the two deflections ($\delta_{thermal}$ - δ_{mech}) will yield the displacement due to the presence of the solder δ_{solder}. In other words, if δ_{mech} was minimal, δ_{solder} was large and implied that the solder was soft and compliant. It is a desired mechanical property of an ideal solder.

Since the SJS assembly was instantaneously subjected to small increment in temperature ΔT, the assembly components will change in dimensions according to their respective coefficients of thermal expansion and hence, the stress-and-strain state was created. The strain must be absorbed elastically by the solder, or the frame's upper beam as described by the term $\tau A / K$, with no plastic strain. Also, the change in elastic displacement is given by $\Delta\tau \bullet t / G(T)$; where *G(T)* is the temperature-dependence shear modulus of the solder, and is given by G(MPa) = 20632 – 37.67T(ºC) [56]. The resultant instantaneous stress change is given by:

$$\Delta\tau = \frac{\Delta L \Delta\alpha \Delta T}{A}\left[\frac{1}{\frac{1}{K}+\frac{t}{AG(T)}}\right] \quad \text{or} \quad \Delta\tau = \frac{Force}{A}.$$

With the calibration relationship listed in Figure 16, the force was found based on solder stain gage reading. The shear strain from the thermal mismatch is accommodated by a combination of elastic and plastic shear strains of the solder, γ_{el} and γ_{pl}, respectively.

$$\gamma_{el} = \frac{\Delta\tau}{G(T)}\ ; \qquad \gamma_{pl} = \gamma_{solder} - \gamma_{el}$$

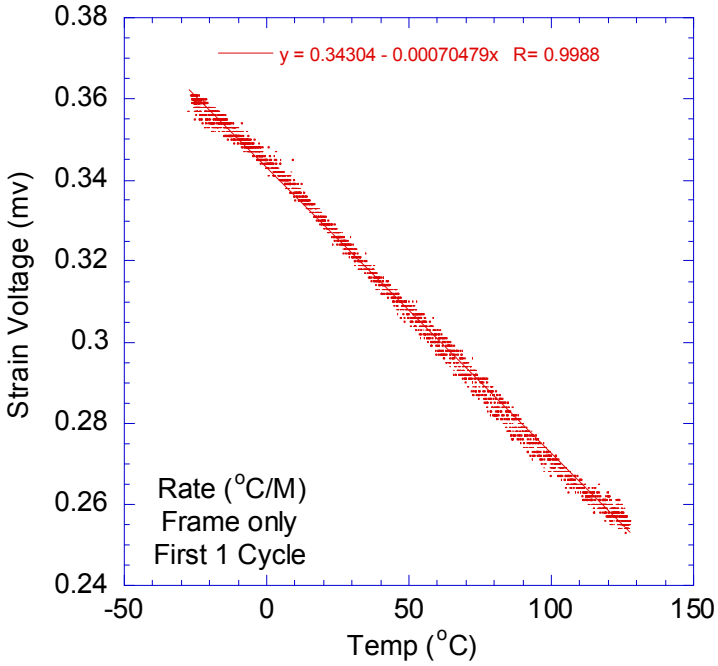

Figure 15. Strain Gage Reading vs Temperature of the Frame only

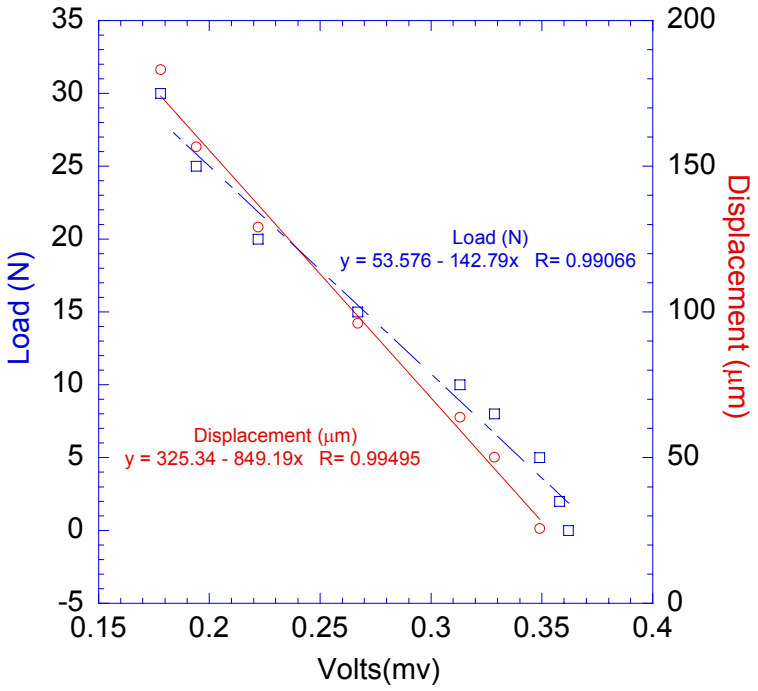

Figure 16. Calibration Curve of Thermal Cycling Frame

THIS PAGE INTENTIONALLY LEFT BLANK

IV. RESULTS AND DISCUSSIONS

A. FABRICATION OF SOLDER JOINTS USING LPS

1. LPS Parameters

In the fabrication process that includes LPS and material preparation and apparatus setup, there were quite a number of challenges that are worth mentioning. They are as follows.

- Environmental control for sintering & storage
- Sintering parameters (applied pressure, temperature and LPS duration)
- Intermetallic compound (IMC) formation

The environmental control against oxidation was crucial as oxidation retarded LPS process. The consequence of oxidation was the formation of indium oxide (In_2O_3) and tin monoxide (SnO). Both oxides have the melting points higher than 1000°C. Indium oxide was broken up during the gentle grinding and deformation in the mortar and pestle, and was incorporated into the molten indium during LPS. Thus, it was not a major issue. However, the sintering temperature was not designed to melt the tin powder. When older stock of tin powder was used, the dark colored oxidized tin powder was not melted even at 400°C even through the melting point of pure tin is 232°C.

Prior to the sintering process, the powder constituting the solder was mixed in an inert gas to minimize oxidation. Since no container offers complete isolation from oxygen in ambient air, the solder slowly oxidizes, which might result in a reduction in wetting. The rate of oxidation is proportional to the exposed surface area of the solder material (powder form), humidity, temperature, time, and available oxygen. The solder material was mixed in a glove box, and used immediately. The leftover was stored in the inert gas (i.e. argon) or in vacuum container to minimize oxidation with an added silica desiccant. In this way, the problem of oxidation was kept to the minimal.

Applied pressure for forming the sample was required for good interface bonding between the copper rods and the solder joint itself. This would translate into good interconnection between the substrate and the solder balls as well as the microchip to the solder balls. The pressure range of 35 MPa was selected for forming a green solder joint. During LPS, the applied pressure was reduced to about 3 MPa to alleviate the problem of loss of molten indium by being squeezed out of the graphite die. The reduced pressure also facilitated particle rearrangement during first stage of the LPS process, and compaction with lower pressure would not even pack the solder well enough and led to large voids for sintering.

The selected sintering temperature was at the region of 162°C. This temperature was enough to melt the indium. This was required for liquid phase sintering with molten indium working around the tin grain boundary.

Sintering for a longer period of time might be beneficial for solution precipitation and grain growth. However, this risks the formation of excessive intermetallic compound (IMC) which would embrittle the solder- copper interference. Furthermore, it was noted that a prolonged sintering time allow absorption of the molten indium into the tins grains, causing de-sintering and swelling. Hence, the total sintering time was kept limited to 2 mins above 160ºC.

2. Microstructure of the Monolithic Solder

Once the sample had been fabricated, it was then placed into the molding material and polished to 0.1 micron surface finish. Next, the microscopic investigation was conducted on the polished sample (Figure 17). The monolithic solder was made of 80Sn-20In sintered (LPS) at 162°C.

Optical microscopy and Scanning Electron Microscopy (SEM) were used to gather the micro-structural images for analysis. Note that due to the proximity of the tin's and indium's atomic numbers in term both have the similar electron energy level, Energy dispersive X-ray spectroscopy (EDS) analysis could not be

performed effectively. Both metals' energy peaks fell around the spot in the spectrum and masking each other's signal.

Figure 18 shows the microscopic image of the solder-copper rod Interface. It was observed that the interface was excellent without sign of crack which was typically depicted a dark black line. This was achievable by sprinkling a small amount of excess indium powder onto the surfaces of the copper rods prior to compaction and LPS.

Figure 19 shows the inner region of the solder. This micro-structure was fairly common across the solder. Very few voids were observed and the micro-structure showed grain boundaries which confirmed well with the adjacent grains. Hence, the LPS process was considered workable.

When the solder (pellet form) was subjected to compression test shown in Figure 20, it was observed that the stress-strain curve of the solder (70Sn-30In) fell in between the tin and indium stress-strain curve. The obtained yield strength was about 7 MPa , which is significantly less than that of tin. This was due to the accommodation of strain by creep and the intergranular indium, allowing the solder to be soft and compliant. Although the tested solder was made of 70v% tin and 30v% indium, the characteristic was very similar to that of the solder (80Sn-20In). solders for which the thermo-mechanical cycling (TMC) data are reported subsequently.

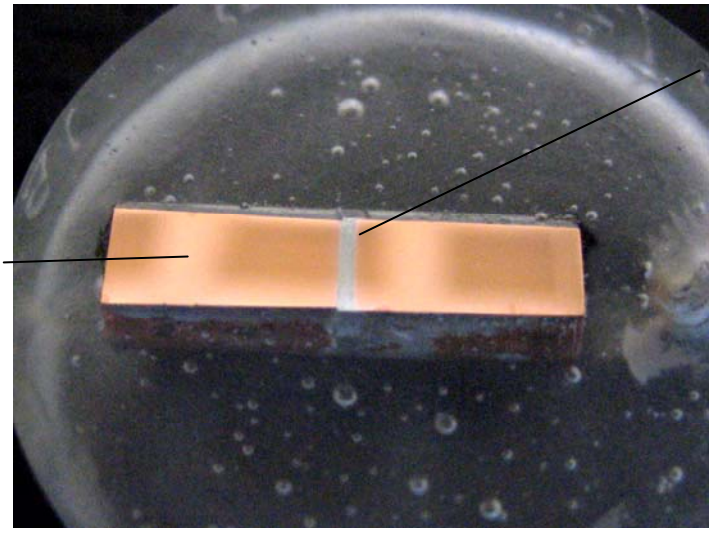

Figure 17. Polished Sample (SJS) in the moulding material for microscopic examination

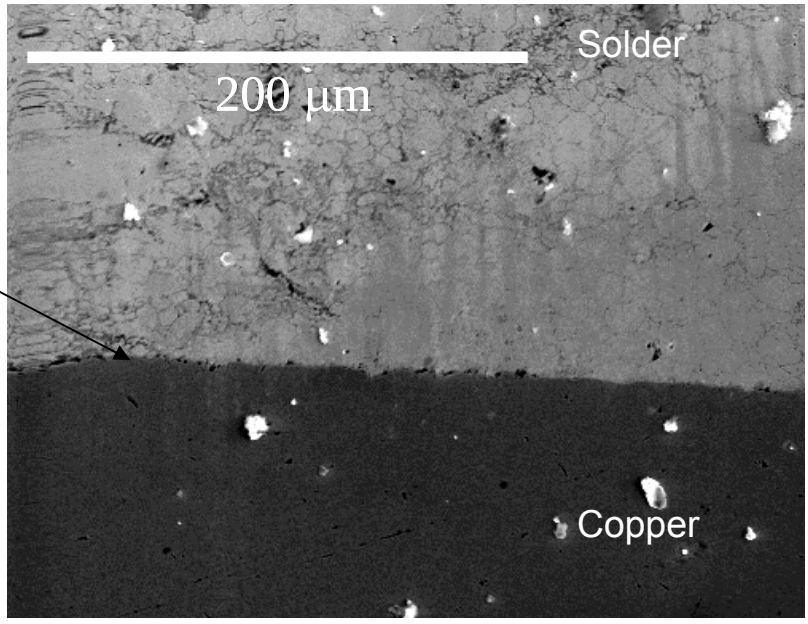

Figure 18. SEM of the Solder- Copper Rod Interface

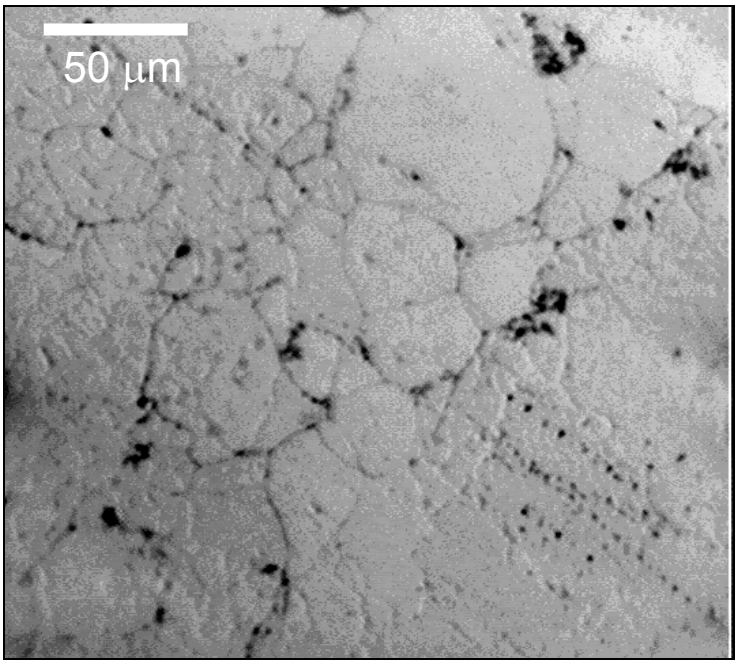

Figure 19. Typical Micro-structure of the monolithic solder

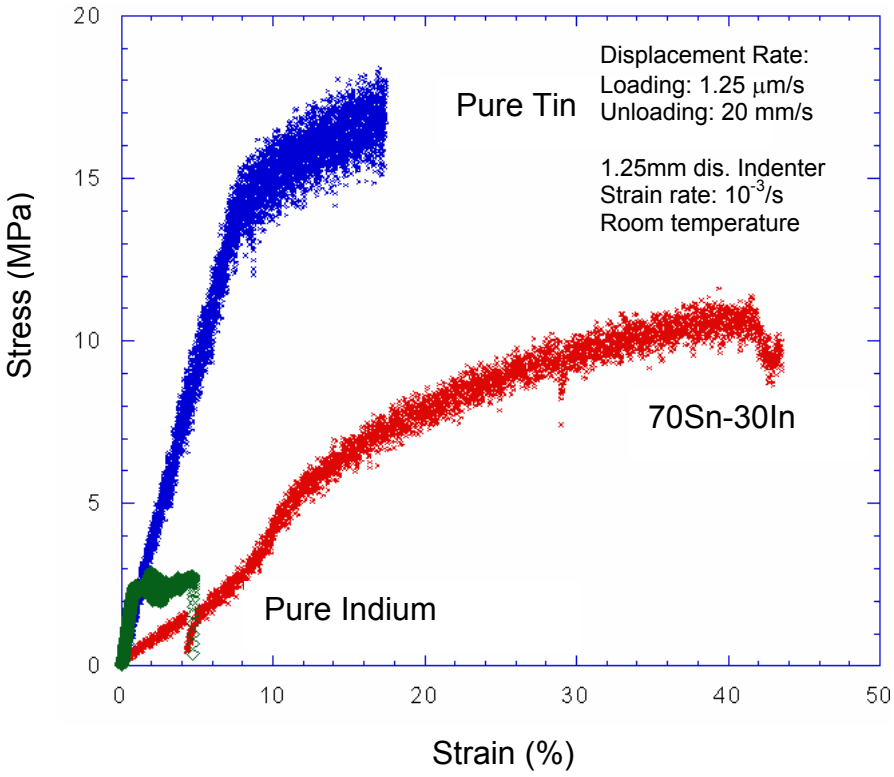

Figure 20. Stress-Strain Curve form Compression Test

3. Microstructure of the Composite Solder

The composite solder was fabricated from the mixed powder of 10v% NiTi particulates and 90v% solder (80Sn-20In). The sintering (LPS) parameters were identical to the monolithic solder fabrication.

The composite solder was generally well packed/pelletized with only a small amount of residual porosity. Figure 21 and Figure 22 show the microscopic images from the SEM. In the figure, it is also shown that the NiTi particulates were quite well distributed in the solder. The grain boundary was not visible even at high magnification.

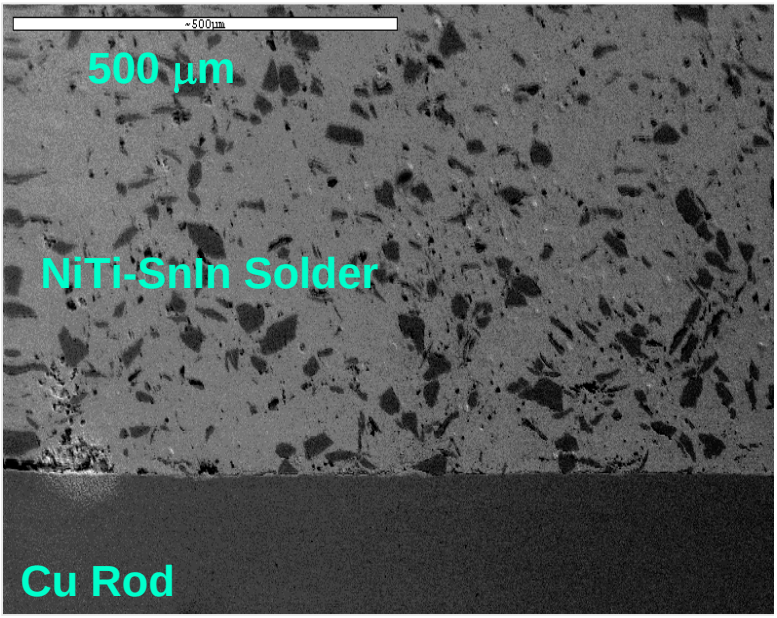

Figure 21. SEM of the interface between the composite solder

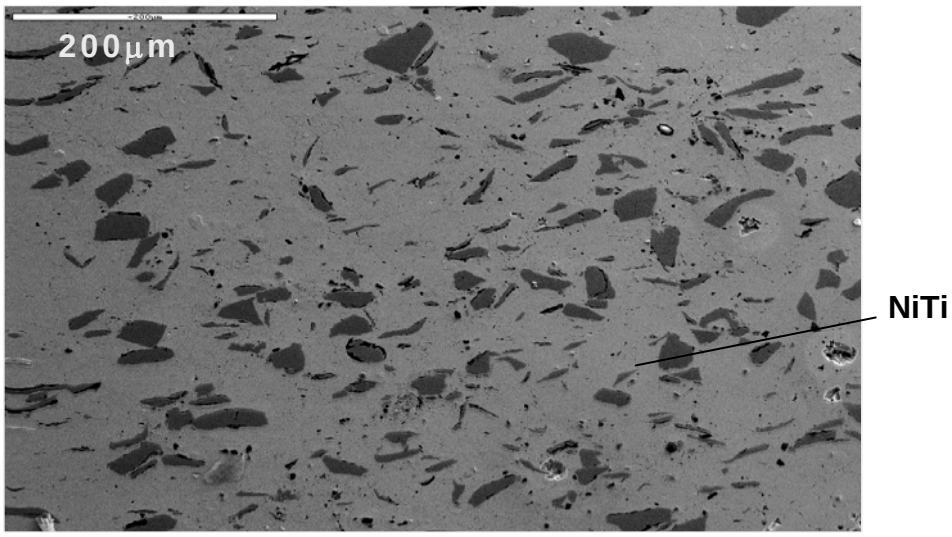

Figure 22. SEM image of the NiTi SMA Particles in the composite solder

B. THERMAL CYCLING TEST RESULTS

The overall diameter of SJS sample was 5.8 mm throughout the length with the solder of 0.2 mm thick. The monolithic solder was subjected to TMC of 99 cycles continuously without failure. Each cycle was lasted for about an hour. The composite solder was also subjected to the same TMC profile for 20 cycles and crack along the solder's cross section was observed. Hence, only the first ten TMC cycles of both monolithic and composite solders were analyzed and discussed here.

Shear stresses developed in the monolithic and composite solder in response to the thermo-mechanical cycling are shown in Figure 23 and Figure 24, respectively. The sample temperatures corresponding to the shear stress values are also plotted in these figures. Figure 25 and Figure 26 show the inelastic shear strains of the monolithic and composite solders, respectively. Thermal strains and mechanical strains (deflection from the top beam of the TMC frame) are also shown in the Figure 25 and Figure 26 for their respective solder types. On all the four figures mentioned above, a typical cycle (-25ºC → +125ºC → -25ºC) which is located in the dashed box is used for discussion and comparison.

The monolithic solder (Figure 23) experienced an increase in shear stress with increasing temperature (heating from room ambient), whereas, the composite solder (Figure 24) reacted differently. When the temperature was increasing from -25ºC to +10ºC, the shear stress response of the composite solder joint was similar to that of the monolithic solder's joint. Once the temperature of the composite solder reaches +10ºC, the solder shear stress dropped by 1.2 MPa and then continued to increase with the increasing temperature. This drop of the shear stress in the composite solder was due to the martensite-to-austenite phase transformation of the reinforced NiTi particulates. In the NiTi powder based in this work, the B19' → B2 transformation occur over 35ºC - 45ºC. However, the stress vs time plots shown in Figure 24 displays a reduction in stress at 20ºC. This is possibly because of a lag in the measured frame temperature relative to the actual temperature of the solder joint. The NiTi particles undergo shape memory recovery from the deformed shape to the original shape when the temperature reaches to B19' → B2 transformation temperature.

The reverse transformation strain in the reinforcements induces a back-stress on the surrounding Sn-In solder matrix, thus reducing the overall shear stress. As a result, the amplitude of the shear stress for monolithic solder was about twice that for the composite solder.

Although the martensite-to-austenite phase transition started at about 35°C as measured by differential scanning calorimetry (DSC), the phase transition for the composite solder was reflected in the figure at somewhat different temperatures (about 20°C). This is because the actual sample temperature lags behind that of the bimetallic-frame, from which the temperature measurements are made. As the TMC frame was heating up, a hotter air was needed to heat the TMC frame to the desired temperature point.

As expected, the accumulation of inelastic strain for the composite solder (Figure 25) was lesser than that of the monolithic solder (Figure 26). The inelastic strain of the monolithic solder was oscillating in the range of 0.8, whereas, that of

the composite solder was oscillating in the range of 0.65. The magnitude of thermal strains was the same for both solders since it was generated from the same TMC frame undergoing the same temperature profile. The mechanical strain refers to the vertical deflection of the top beam of the TMC frame in response to the solder's shear strain, and is therefore dependent on the properties of the joint material. Clearly, the observation that the inelastic strain range is smaller in the composite solder suggests that the mechanical strains in the monolithic solder are larger. [Note that the total joint strain ≈ (thermal strain – mechanical strain), which is almost equal to the total inelastic strain]. This is because the large stress induced in the monolithic joint induces a large amount of creep and plasticity, particularly near to high and low temperature ends of the thermal cycle.

The back-stress generated by the B19' → B2 transformation alleviates these strains, and therefore is expected to improve the low cycle fatigue life of the solder joint.

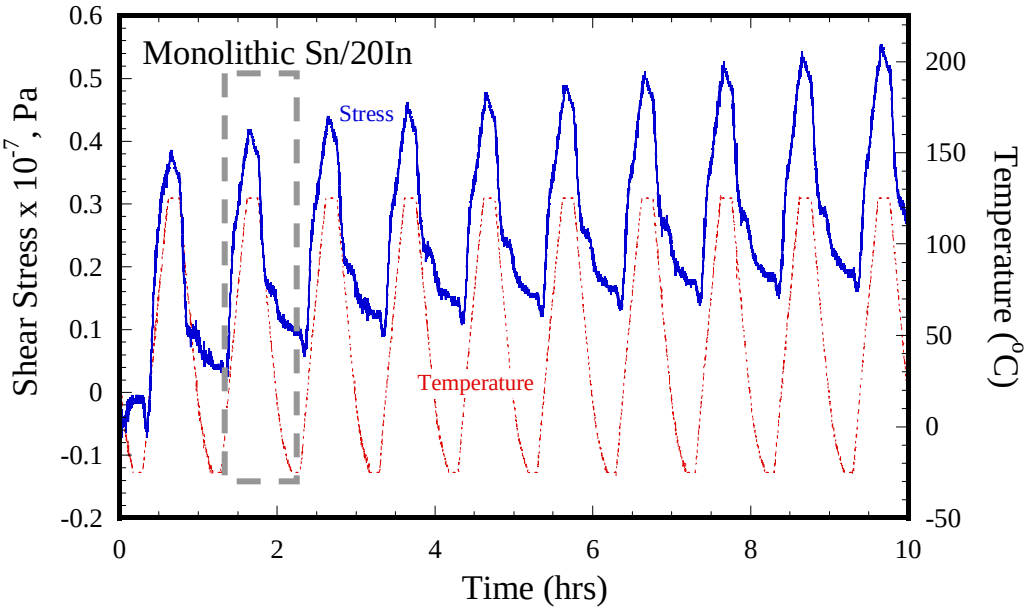

Figure 23. Monolithic Solder Joint's Shear Stress

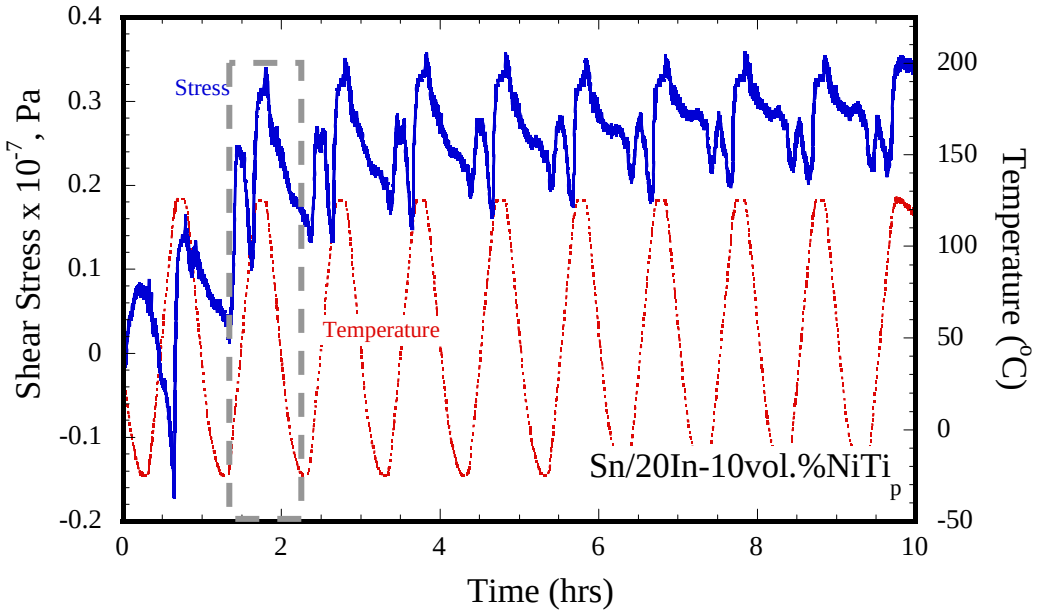

Figure 24. Composite Solder Joint's Shear Stress

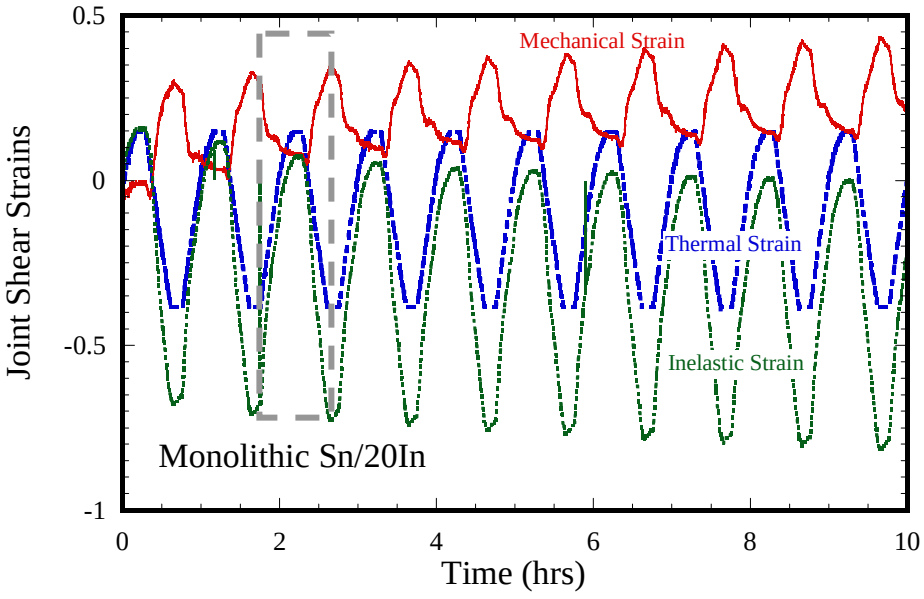

Figure 25. Monolithic Solder Joint's Shear Strains

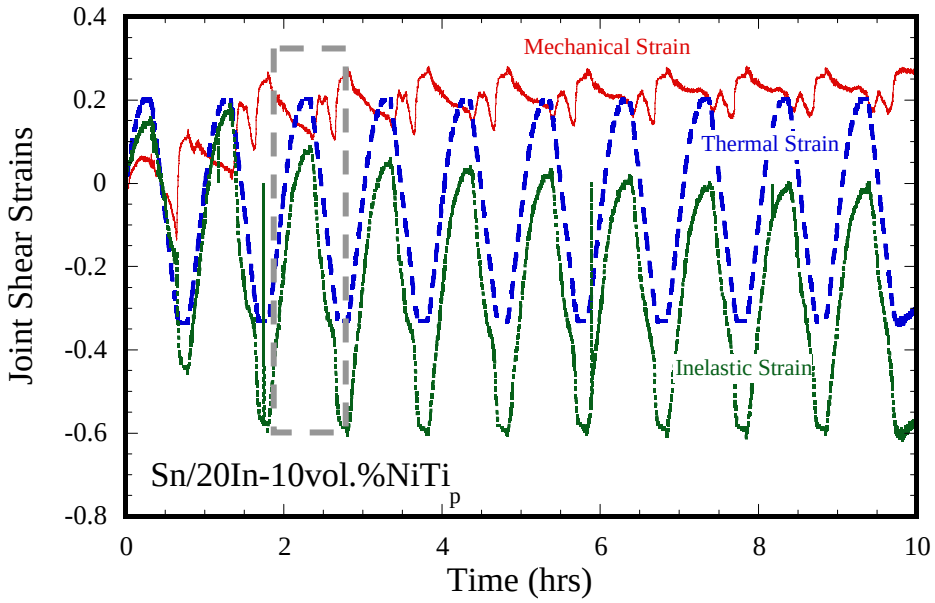

Figure 26. Composite Solder Joint's Shear Strains

THIS PAGE INTENTIONALLY LEFT BLANK

IV. CONCLUSION

In this project, a new fabrication process of incorporating NiTi particles in a solder matrix in the solid state has been developed. This has been accomplished by liquid phase sintering of tin with a small amount of indium powder (20-30 vol.%), and the requisite amount of NiTi (10 vol. %)

The thermo-mechanical behavior of the smart composite solder (80Sn-20In), reinforced with a NiTi-based Shape-Memory Alloy particulates [10v% NiTi 90v% (80Sn-20In)] had been investigated in comparison with its monolithic solder. The experiments on thermo-mechanical cycling of solder joints showed that the shape memory effect was observed in the composite solder joint during heating. The experimental data collected from the thermo-mechanical cycle between -25 ºC and 125ºC with a ramp rate of 7.5ºC / min, were analyzed to obtain the shear stress and the inelastic strain of the solders.

The thermo-mechanical experiments on the composite solders showed the solders reinforced with NiTi particulates significantly decrease the inelastic strain range during thermal cycling. As the NiTi particles deform in shear concurrently with the solder during the thermal cycling, it undergoes martensite-to-austenite (M→A) transformation, placing the solder next to the reinforcements in reverse shear. This transformation results in a back-stress, and thus reduces stresses within the solder in the immediate neighborhood of the particles. The reduced stress reduces the total creep/ inelastic strains accrued, and hence is likely to enhance the low cycle fatigue life and the composite as compared with the monolithic solder.

THIS PAGE INTENTIONALLY LEFT BLANK

ENDNOTES

1 Frear, D. R., Dennis Grivas, and J. W. Morris Jr., “Thermal Fatigue in Solder Joints,” Journal of Metals, pp. 18-22, June 1988.

2 Lee, Y. G., J. G. Duh, “Characterizing the Formation and Growth of Intermetalic Compound in the Solder Joint,” Journal of Material Science, 33, pp. 5569-5572, 1998.

3 Frear, D. R., Dennis Grivas, and J. W. Morris Jr., “A Microstructural Study of the Thermal Fatigue failures of 60Sn-40Pb Solder Joints,” Journal of Electronic Materials, Vol. 17, No. 2, pp. 171-180, 1998.

4 Hacke, P., A. Sprecher, and H. Conrad, “Microstructure Coarsening During Thermo-Mechanical Fatigue of Pb-Sn Solder Joints,” Journal of Electrinic Materials, Vol. 26, No. 7, 1997.

5 Conrad, H., Z. Guo, Y. Fahmy, and Di Yang, “Influence of Microstructure Size on the Plastic Deformation Kinetics, Fatigue Crack Growth Rate, and Low Cycle Fatigue of Solder joints,” Journal Of Electronic Materials, Vol. 28, No. 9, 1999.

6 Hacke, P. L., Y. Fahmy, and H. Conrad, “Phase Coarsening and Crack Growth Rate During Thermo-Mechanical Cycling of 63Sn-37Pb Solder Joints,” Journal of Electronic Materials, Vol. 27, No. 8, 1998

7 Mavoori H. and S. Jin, J. Electron, Mater. 27, 1216 (1998).

8 Frear, D. R., “The Mechanical Behavior of Interconnect Materials for Electronic Packaging,” JOM, pp. 49-53, May 1996

9 Masazumi Amagai et al, “Mechanical Characterization of Sn-Ag-based Lead-Free Solders,” Microelectronics Reliability, Vol. 42, pp. 951-966, 2002.

10 Wang Z. X., I. Dutta, and B.S. Majumdar, Thermo-mechanical response of a Novel Adaptive Lead-Free Solder System, Scripta Materialia, November 2003.

11 J. D. Van Wyk and F. C. Lee, “Power electronics technology--status and future,” in Proc. Virginia Power Electron. Center Sem., 1999.

12 Zaheed S. Karim, Lead-Free Solder Bump Technologies for Flip-Chip Packaging Applications, Advanced Packaging Technology Conference Proceedings Articles, 06/12/2001.

13 Subramanian K. N., T. R. Bieler, and J. P. Lucas, Micro structural Engineering of Solders, Journal of Electronic Materials, Vol. 28, No.11, 1999.

14 T. Takemoto, Introduction of JIS Related Lead-Free Solder and Soldering, IEEE 2005 6th International Conference on Electronics Packaging Technology, 2005.

15 Pb-Free Solder Fabrications, Indium Corporation of America

16 Nordwall, B., “Air Force Links Radar Problems to Growth of Tin Whiskers”, Aviation Week and Space Technology, June 20, 1986, pp. 65-70

17 K.J. Heutel, "Problem Notification - Tin Whisker Growth in Electronic Assemblies," GIDEP Alert F3-A-87-04A, February 19, 1988.

18 I. Dutta, B.S. Majumar, D. Pan, WS Horton, W. Wright and Z.X. Wang, Development of a Noval Adaptive Lead-Free Solder Containing Reinforcements Displaying the Shape-Memory Effect, Journal of Electronic Materials, vol 33, no 4, 2004

19 C.L. Yu, S.S. Wang, and T.H. Chuang, Journal of Electronics Materials, 31, 5, May 31 2002.

20 P Geng, el at, Alternative Lead-free Solder Joint Integrity Under Room Temperature Mechanical Load, ITHERM 2004

21 J.W. Morris, Jr., J.L. Freer Goldstein, and Z. Mei, "Microstructure and Mechanical Properties of Sn-In and Sn-Bi Solders" (Overview), J. of Materials, July 1993, pp. 25-27.

22 Victoria Bhattacharya, K. Chattopadhyay, Morphology and phase transformation of nanoscaled indium–tin alloys in aluminium, Materials Science and Engineering, A 375–377 (2004) 932–935.

23 Seong-Yong Hwang et al, “Microstructure of Lead-Free Composite Solder Produced by an In-Situ Process,” Journal of Electronic Materials, Vol. 31, No. 11, pp. 1304-1308, 2002.

24 McDougall, J., S. Choi et al, “Quantification of Creep Strain Distribution in Small Crept Lead-Free In-Situ Composite and Non-Composite Solder Joints,” Materials Science and Engineering, A285, pp. 25-34, 2000.

25 C. G. Kuo et al, “Creep-Fatigue Life Prediction of In-Situ Composite Solder Joints,” Metallic Materials Transactions, 26A, pp. 3265-3272, 1995.

26 J.L. Marshall and J. Calderon, Solder. Surf. Mount Technol. 9, 22 (1997).

27 A.W. Gibson, K.N. Subramanian, and T.R. Bieler, J. Adv. Mater. 30, 19 (1998).

28 K.N. Subramanian, T.R. Bieler, and J.P. Lucas, J. Electron. Mater. 28, 1176 (1999).

29 C.G. Kuo, S.M.L. Sastry and KL Jerina, Mater. Trans. A 26A, 3265, 1995.

30 Guo F., S. Choi, J. P. Lucas and K. N. Subramanian, Solder surface Mount Technnology 13, 7 (2001).

31 Guo F., J. Lee, S. Choi, J. P. Lucas, T. R. Bieller and K. N. Subramanian, J. Electron. Mater. 30, 1073 (2001).

32 Evangelos Fountoukidis, Master of Science Thesis, Thermo-mechanical Reponse of Monolithic and NiTi Shape Memory Alloy Fiber Reinforced Sn-3.8Ag-0.7Cu Solder, Naval Postgraduate School, September 2005.

33 I. Dutta, B.S. Majumdar, D. Pan, W.S. Horton, W. Wright, Z.X. Wang, J. Electronic Mater. 33, 258 (2004).

34 Z. X. Wang, I. Dutta and B.S. Majumdar, Scripta Mater., 54, 627 (2006).

35 Z. X. Wang, B.S. Majumdar and I. Dutta, Mater. Sci. Eng. A, 421, 133 (2006)

36 D. Pan, I. Dutta, S. Ma, B.S. Majumdar and S. Harris, J. Electronic Mater., 35, 1902 (2006).

37 Hodgson Darel E., Shape Memory Applications, Inc., Ming H. Wu, Memry Corporation and Robert J. Biermann, Harrison Alloys, Inc., Shape Memory Alloys.

38 The Nickel Industrial titanium innovative group, http://www.nitig.ch/9081.html, visited 11/11/2006

39 Silvain J. F., J. Chazelas, M. Lahaye S. Trombert, The Use of Shape Memory Alloy NiTi particles in SnPbAg matrix: interfacial chemical analysis and mechanical characterization, Materials Science and Engineering A273-275 (1999) 818-823.

40 Dutta I., B. S. Majumdar, D. Pan, W. S. Horton, W. Wright and Z. X. Wang, Development of a Novel Adaptive Lead-Free Solder Containing Reinforcements Displaying the Shape Memory Effect. Journal of Electronic Materials, Vol. 33, No. 4, 2004.

41 C. Val, M. Leroy, and H. Boulharts, Proc. Int. Conf. Electron. Technol. (Windsor, UK: 1994), pp. 119–122.

42 S. Trombert, J. Chazelas, P. Bonniay, W. Van Moorleghem, M. Chandrasekharan, and J.F. Silvain, Proc. SPIE. Int. Soc. Opt. Eng. Vol. 2779 (Bellingham, WA: SPIE, 1996), pp. 475–480.

43 S. Trombert, J. Chazelas, M. Lahaye, and J.F. Silvain, Compos. Interfaces 5, 479 (1998).

44 J.F. Silvain, J. Chazelas, M. Lahaye, and S. Trombert, Mater. Sci. Eng. A 273–275, 818 (1999).

45 J.F. Silvain, J. Chazelas, and S. Trombert, Proc. Shape- Memory Superelastic Technology (New York: John Wiley & Sons, 2002), Vol. 7, pp. 128.

46 O. Fouassier, S. Trombert, J.F. Silvain, J. Chazelas, D. Aslandis, A. Serneels, and W. Van Moorleghem, Proc. Shape-Memory Superelastic Technology (Materials Park, OH: SMST, 1999), pp. 1–9.

47 ZX Wang, I Dutta, BS Majumdar, Thermal Cycle Response of a Lead-Free Solder Reinforced with Adaptive Shape Memory Alloy, Scripta Mater, 54, 627 (2006).

48 I. Dutta, D. Pan, S. Ma,1 B.S. Majumdar, And S. Harris, Role of Shape-memory Alloy Reinforcements on Strain,Evolution in Lead-free Solder Joints, Journal Of Electronic Materials, Vol. 35, No. 10, 2006

49 SF Corbin, Alternative Processing of Solder Pastes Using Transient Liquid Phase Sintering (TLPS), Workshop on Lead-Free Reliability, Centre for Microelectronics Assembly and Packaging, 5/22/02.

50 Randall M German, Sintering Theory And Practice, John Wiley & Sons,1996.

51 D. Gupta, G. Soman, S. Dev, Thiourea, a convenient reagent for reductive cleavage of olefin ozonolysis products, “Tetraedron”, 38, 3013 (1982).

52 I. Dutta, A. Gopinath and C. Marshall, Journal of Electronic Materials, Vol. 31, No. 4, 2002.

53 Hacke Peter L., Arnold F. Sprecher, and Hans Conrad, Modeling of the thermomechanical fatigue of 63Sn37Pb alloy, ASTM STP 1186, Sehitoglou, Ed., American Society for testing and Materials, Philadelphia, 1993, pp. 91-105.

54 Choi S., K. N. Subramanian and T. R. Bieler, Characterization of the Growth of Intermetallic Interfacial Layers of Sn-Ag and Sn-Pb Eutectic Solders and their Composite Solders on Cu Substrate During Isothermal Long-Term Aging, Journal of Electronic Materials, Vol. 28, No.11, 1999.

55 John G. Bai, Jesus N. Calata, and Guo-Quan Lu, “Comparative Thermal and Thermomechanical Analyses of Solder-Bump and Direct- Solder Bonded Power Device Packages Having Double-Sided Cooling Capability” 0-7803-8270-6/04/2004 IEEE

56 P.T. Vianco, J.A. Rejent, A.C. Kilgo, Journal of Electronic Materials, 32, (2003) 142.

THIS PAGE INTENTIONALLY LEFT BLANK

INITIAL DISTRIBUTION LIST

1. Defense Technical Information Center
   Ft. Belvoir, Virginia

2. Dudley Knox Library
   Naval Postgraduate School
   Monterey, California

3. Professor Indranath Dutta
   Naval Postgraduate School
   Department of Mechanical & Astronautical Engineering
   Monterey, California

4. Distinguished Professor Anthony J. Healy
   Chairman, Department of Mechanical & Astronautical Engineering
   Naval Postgraduate School
   Monterey, California

5. Professor Yeo Tat Soon
   Director, Temasek Defence Systems Institute (TDSI)
   National University of Singapore
   Singapore

6. Ms Tan Lai Poh
   Senior Administration Officer
   Temasek Defence Systems Institute (TDSI)
   National University of Singapore
   Singapore